Novel Concepts for Light Management in Flexible Photovoltaics Final Report

by

Dr. Ethan Klem, Prof. Michael Dickey, Dr. Jay Lewis

DEFENSE TECHNICAL INFORMATION CENTER

Information for the Defense Community

DTIC® has determined on 8/4/2014 that this Technical Document has the Distribution Statement checked below. The current distribution for this document can be found in the DTIC® Technical Report Database.

☒ **DISTRIBUTION STATEMENT A.** Approved for public release; distribution is unlimited.

☐ **© COPYRIGHTED.** U.S. Government or Federal Rights License. All other rights and uses except those permitted by copyright law are reserved by the copyright owner.

☐ **DISTRIBUTION STATEMENT B.** Distribution authorized to U.S. Government agencies only (fill in reason) (date of determination). Other requests for this document shall be referred to (insert controlling DoD office).

☐ **DISTRIBUTION STATEMENT C.** Distribution authorized to U.S. Government Agencies and their contractors (fill in reason) (date determination). Other requests for this document shall be referred to (insert controlling DoD office).

☐ **DISTRIBUTION STATEMENT D.** Distribution authorized to the Department of Defense and U.S. DoD contractors only (fill in reason) (date of determination). Other requests shall be referred to (insert controlling DoD office).

☐ **DISTRIBUTION STATEMENT E.** Distribution authorized to DoD Components only (fill in reason) (date of determination). Other requests shall be referred to (insert controlling DoD office).

☐ **DISTRIBUTION STATEMENT F.** Further dissemination only as directed by (insert controlling DoD office) (date of determination) or higher DoD authority.

Distribution Statement F is also used when a document does not contain a distribution statement and no distribution statement can be determined.

☐ **DISTRIBUTION STATEMENT X.** Distribution authorized to U.S. Government Agencies and private individuals or enterprises eligible to obtain export-controlled technical data in accordance with DoDD 5230.25; (date of determination). DoD Controlling Office is (insert controlling DoD office).

Novel Concepts for Light Management in Flexible Photovoltaics Final Report

Drs. Ethan Klem[†] and Jay Lewis[†], Prof. Michael Dickey[‡],
RTI International[†] and NC State University[‡]
Research Triangle Park and Raleigh, NC

Prepared for
Steven Tucker, NSRDEC

2/24/2011

RTI International
3040 Cornwallis Rd
Box 12194
Research Triangle Park, 27709

20110719147

ABSTRACT

This one year project explored novel concepts for light management in light weight, flexible solar cells by engineering surface topography to enhance the overall efficiency of photovoltaic (PV) devices. During the project methods were developed to enable the fabrication of PV substrates with corrugated, buckled surfaces formed by thermal, mechanical, and chemical processes. These substrates were then used in the fabrication of PV devices based upon thin film small molecule organic materials and thin film solution processed quantum dot materials; two emerging technologies with inherently low cost and scalable manufacturing methods. This allowed us to demonstrate that high surface area topographies can increase light absorption in thin film PV devices and lead to increased performance by enhancing the devices' ability to harvest incident light.

CONTENTS

List of Figures

List of Tables

1. PROJECT SUMMARY

This collaborative RTI-NCSU one-year program explored novel concepts for light management in light weight, flexible solar cells by engineering surface topography in an effort to enhance the overall efficiency of photovoltaic devices. The concepts utilized surface instabilities that produced hierarchically corrugated surfaces on the nanometer scale without lithographic patterning. The concepts are applicable to all thin-film photovoltaic technologies and are particularly well-suited for mechanically flexible, low-cost systems. The project focused on developing techniques for generating corrugated surfaces on substrates suitable for photovoltaic device processing and then on applying these substrates to the fabrication of thin film photovoltaic devices. The two photovoltaic device technologies that were focused upon were organic photovoltaics (OPVs) and quantum dot photovoltaics (QDPVs).These are appealing technologies for their low-cost and compatibility with flexible substrates. These technologies have a common feature; relatively short charge transport lengths require devices with thin active regions for efficient charge separation, but thin-films are incapable of absorbing all of the incident sunlight. As such, each these thin-film technologies would benefit from an increase in the efficiency of their capture of sunlight. The RTI-NCSU team explored this hypothesis by integrating surface corrugation science with substrates compatible with the fabrication of thin film PV devices. The substrates were then used to fabricate OPV and QDPV based devices. Finally the most promising substrate and device technologies were scaled up in size.

Major accomplishments over the course of this project include:

- Fabricated PV substrates with corrugated, buckled surfaces formed by thermal, mechanical and chemical processes.
- Increased aspect ratio of the buckles to favor improved light absorption.
- Measured the optical absorbance of buckled topology substrates with various geometries and compared them to planar devices as well as topography replicated from commercial Si solar cells.
- Demonstrated conclusively that buckles improve light absorption.
- Fabricated small molecule OPV device on mechanically and thermally buckled substrates.
- Established effective processing steps to fabricate crossbar device configuration to improve reliability of electrical contacts.
- Repeatedly demonstrated buckled OPV devices that showed significant increase in harvested photocurrent over their planar equivalent.
- Fabricated a champion buckled device with a power conversion efficiency enhancement of 21% and harvested short circuit photocurrent enhancement of 68%.

- Explored chemical treatment/processing methods for improving performance of Quantum Dot PV devices. Developed air annealing process that increased QDPV power conversion efficiency from 1.56% to 2.24%, an increase of 43%.
- Demonstrated performance impact of using thermally buckled substrates to fabricated QDPV devices and observed an 11% increase in the harvest short circuit photocurrent over a planar equivalent.
- Scaled up device size and fabricated OPV devices on planar and thermally buckled topography substrates with active areas of 50 cm^2.

2. PROGRESS TOWARDS PROJECT TASKS

The project was subdivided to include five distinct tasks. Table 1 summarizes the status of these tasks and highlights some of the specific accomplishments that were achieved during work on each of these tasks. Section 0 of the report expands on this table and details specifics of the efforts that made up each of the larger tasks.

Table 1. Summary of the progress made on project deliverables and milestones.

Task	Status	Highlights
Design and synthesis of PV substrates with hierarchically corrugated surfaces	Complete	Fabricated PV substrates with corrugated, buckled surfaces formed by thermal, mechanical and chemical processes. Increased aspect ratio of the buckles to favor improved light absorption. Developed a quantitative protocol for characterizing buckle wavelength. Explored the use of e-field to create buckles with the goal of increasing aspect ratio. Investigated solvent swelling as a way to control buckle geometry. Optimized the processes used to pattern the electrodes for better electrical contact. Performed optical modeling of the integrating sphere used for optical measurements. Measured the optical absorbance of buckled substrates with various geometries and compared it to planar devices as well as topography replicated from commercial Si solar cells.
Demonstrate improved light harvesting using small-molecule OPV devices	Complete	Fabricated small molecule OPV device on mechanically and thermally buckled substrates. Resolved challenges associated with making electrical contact to buckled topology devices. Studied issues that lead to initially poor performance and low yield of buckled OPVs. Identified and resolved problems with low fill factors and short circuits in devices made on in-house deposited ITO. Repeatedly demonstrated buckled OPVs that showed

Task	Status	Highlights
		significant increase in harvested photocurrent over their planar equivalent. Fabricated buckled OPV devices that showed an increase in power conversion efficiency over that of their planar equivalent. Champion buckled device had power conversion efficiency enhancement of 21% and harvested short circuit photocurrent enhancement of 68%.
Demonstrate improved light harvesting using QDPVs	Complete	Fabricated QDPV devices which compared the performance of dot-contact and crossbar contact device geometries. Developed new fabrication methods for depositing solution processed QDs onto thermally buckled PS substrates. Fabricated QDPV device with thermally buckled PS substrates that exhibited an 11% increase in the harvested short circuit photocurrent over a planar equivalent.
Enhance QDPV performance using chemical methods	Complete	Explored chemical treatment/processing methods for improving performance of Quantum Dot PV devices. Demonstrated that air annealing increased QDPV power conversion efficiency from 1.56% to 2.24%, an increase of 43%.
Scale-up PV device size	Complete	Fabricated OPV devices on planar and thermally buckled topography substrates with active areas of 50 cm^2.

3. TECHNICAL DETAILS

3.1. Design and synthesis of PV substrates with hierarchically corrugated surfaces

3.1.1. Highlights

- Fabricated PV substrates with corrugated, buckled surfaces formed by thermal, mechanical and chemical processes
- Increased aspect ratio of the buckles to favor improved light absorption

- Developing a quantitative protocol for characterizing buckle wavelength
- Explored the use of e-field to create buckles with the goal of increasing aspect ratio
- Investigated solvent swelling as a way to control buckle geometry
- Performed optical measurements to compare the absorption of buckled topographies to planar topographies
- Optimized the processes used to pattern the electrodes for better electrical contact
- Performed optical modeling of the integrating sphere used for optical measurements
- Measured the optical absorbance of buckled substrates with various geometries and compared it to planar devices as well as topography replicated from commercial Si solar cells.

3.1.2. Fabrication and Characterization of Corrugated Surfaces

The premise of this project was to build thin film photovoltaics on corrugated substrates. We therefore spent considerable time mastering the fabrication and replication of corrugated surfaces using several techniques. The substrates typically consisted of indium tin oxide (ITO) films supported by polymer or polymer / glass. ITO is the standard transparent, conductive electrode used in most opto-electronic devices.

An important aspect of PV fabrication is the deposition of high quality ITO films. ITO is a notoriously difficult material to deposit effectively at low temperatures and the quality depends on a large parameter space. We refined our processing and characterized the films resulting from our best process. Figure 1 is an atomic force micrograph of ITO films formed in our laboratory. These films have low resistivity ($1.5 \times 10^{-3}\ \Omega$ cm, as measured by a 4-point probe) and low roughness (~ 1 nm RMS, as measured by AFM). As expected, the resistivity decreases during post-deposition annealing (at 350 °C), although annealing may not be a processing option depending on the choice of substrate material.

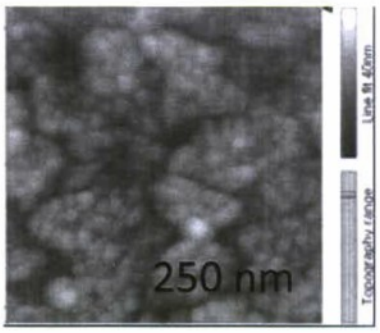

Figure 1. An AFM image of the surface of an ITO film deposited at NCSU. The surface is smooth, highly conductive, and transparent.

Once we established a reliable ITO deposition process, we sought to use it for buckling. Buckling occurs when a rigid film is compressed by an underlying elastic substrate. The buckling wavelengths represent a tradeoff between the bending of the rigid film and the elastic stress relaxation of the underlying substrate. We explored two methods of buckling: (1) building a device on a stretched substrate and subsequently releasing the strain ("mechanical buckling"), and (2) building a device upon a thin film supported by a rigid substrate ("thermal buckling", which arises from thermal stresses during heating). We explored pre-buckled substrates (i.e., those buckled before device fabrication) as well as post-buckled substrates (i.e., those buckled after deposition of the PV materials).

We established techniques to produce mechanically-induced buckles (oxide films on polydimethylsiloxane, PDMS) over 1 x 1" areas. Buckles form by stretching a PDMS substrate, oxidizing the surface (or depositing ITO), and releasing the strain. Figure 2 is a picture of a buckled PDMS substrate. We also developed a method to replica mold (i.e., transfer) these buckled substrates into other materials such as thiol-enes and epoxies. This replica process allowed us to produce topographically identical substrates rapidly. It also allowed us to leverage the soft properties of the PDMS for buckle formation, but use more rigid substrates for PV devices. The replicas are formed by casting and curing a pre-polymer over the buckled surface.

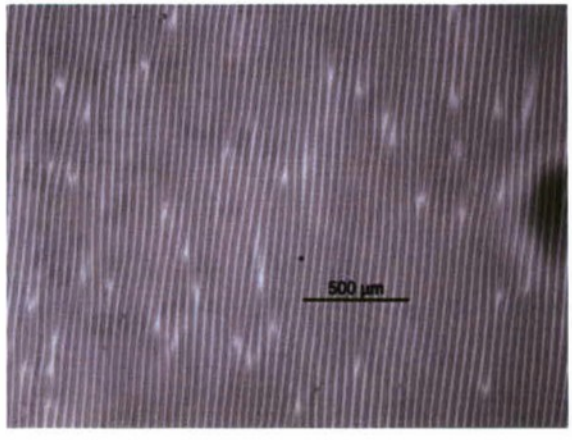

Figure 2. A top-down optical micrograph of buckles produced by mechanically induced buckling.

We had little success building PV devices on PDMS. PDMS is so soft and flexible that the ITO would crack during handling. We also had little success building PVs on top of rigid replicas of mechanical buckles. We believe that shunts formed through the devices due to the roughness of the substrates and the relatively thin active layers deposited over these rough surfaces. Regardless, we spent a significant amount of time trying to make devices from mechanical buckles because they provided the largest aspect ratios (defined as the amplitude of the buckles divided by the wavelength). We hypothesized

that larger amplitude would be required to harvest light effectively. We later found that thermal buckles were sufficient to capture light and also easier to fabricate, so the latter portion of the project focused in this area.

Thermally induced buckling is a relatively newer and less explored approach to creating surface topography than mechanical buckles, but preliminary results showed an encouraging path towards a process that is compatible with device fabrication. For example, Figure 3 shows atomic force microscopy (AFM) images of the topography that resulted from sputtering and subsequent annealing of indium-tin oxide (ITO) films on a layer of polystyrene (PS). Upon heating, the polymer layer causes buckling in the ITO layer due to a variety of factors, such as inherent film stress and a mismatch between the coefficients of thermal expansion. An advantage of the thermally-induced buckling approach is that the ITO films can simultaneously serve as the transparent conductive electrode layer in a photovoltaic device and induce buckling.

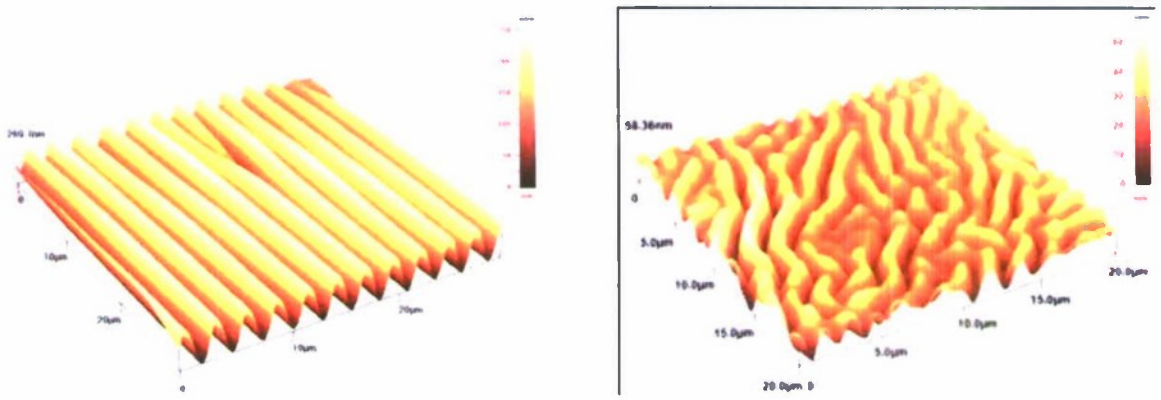

(a) (b)

Figure 3. Representative AFM images of buckled topography produced by depositing and annealing ITO films on a polymer layer. (a) Mechanical buckles produce anisotropic (i.e., oriented) buckles, whereas (b) thermal buckles produce randomly oriented buckles.

We have observed substantial gains in current in OPV devices fabricated on thermally buckled substrates relative to planar substrates (described in Section 3.2.3). We created crossbar devices that consisted of a film stack comprising Corning borosilicate glass, 200 nm ITO and 200 nm of Ag (the buckled substrates included a layer of polystyrene between the glass and ITO). Note that the patterned Ag film is used to reduce series resistance of the crossbar pattern and is not part of the device stack. The important steps from the procedure are listed below:

1. Clean glass by thorough IPA/DI water rinsing, then UVO for 10 min.
2. PS layers (1.5micron thick) introduced via spin casting.
3. PS layers annealed on hot stage at 110°C for 3 hrs.
4. Sputter ITO (34 min at 30W; 4 mTorr, yielding 200nm).
5. Upon ITO sputtering, rinse glass/PS substrates with IPA.
6. In some cases, the ITO was UVO-treated for 10 min.
7. 200nm Ag was deposited on portions of the ITO.

Figure 4 is an image of a patterned glass slide formed using this process. A second device layout was used for devices fabricated at NCSU and can be seen in Figure 6.

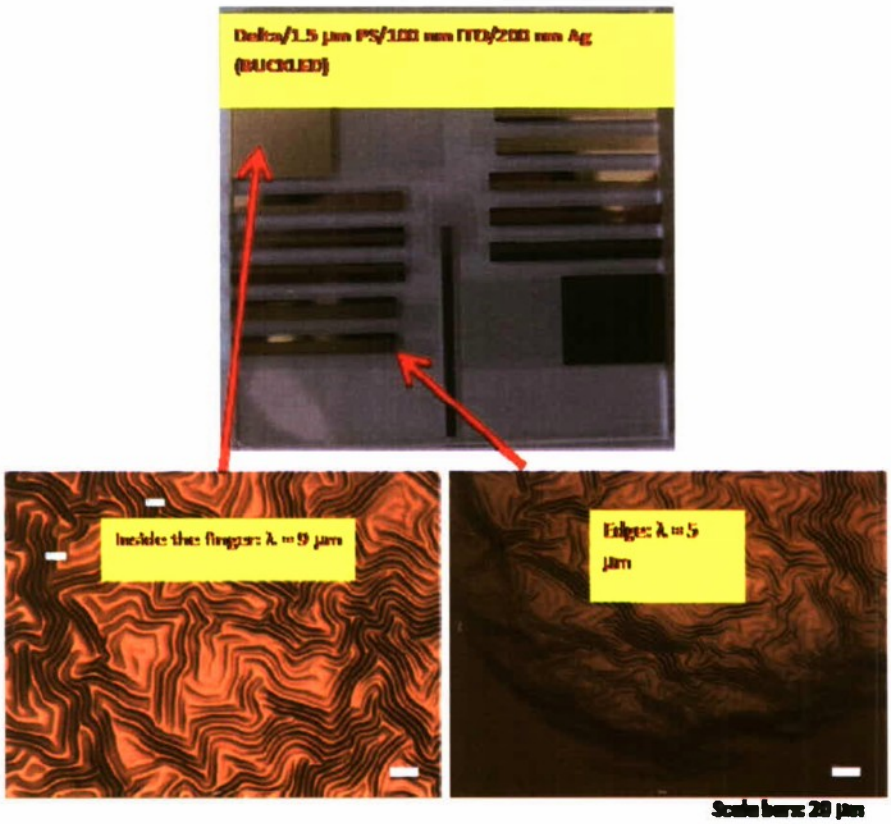

Figure 4. A photograph (top) and micrographs (bottom) of our patterned and buckled ITO electrodes required for the cross bar lay-out described in Section 3.2.3.

The ability to control buckle geometry is important for light harvesting. We studied the role of the substrate (composition and thickness) and film thickness in controlling the periodicity of the buckles. Interestingly, the periodicity appears to vary with thickness for

certain types of substrates (polystyrene), but not others (PDMS). For example, Figure 5 is a plot of wavelength versus substrate thickness for 40 nm films of ITO on polystyrene. The wavelength increases with film thickness.

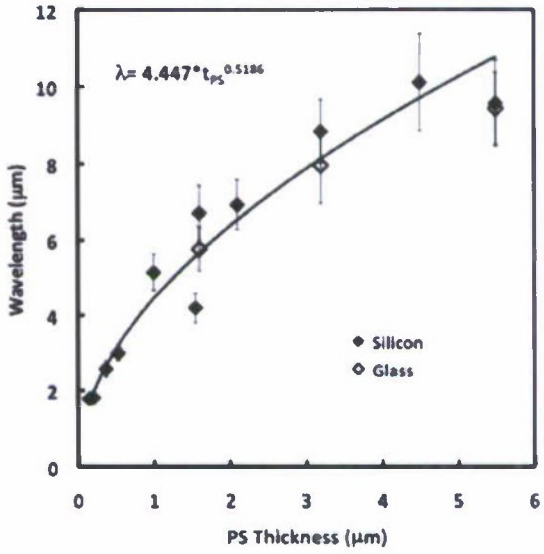

Figure 5. A plot of buckle wavelength versus film thickness for 40 nm ITO films on polystyrene (PS). Other substrates, such as PDMS, do not show this correlation.

Once we determined how to reliably make buckles, we sought to make OPV devices. We spent time optimizing our process to get the best films possible. We found that poor film quality of the active layer of the OPV contributes to irreproducibility and low efficiencies. By varying the conditions used to cast the films, we improved the quality (homogeneity) of the films. We made devices with films using improved processing conditions, as shown in Figure 6.

We also formed devices on buckled substrates. Figure 7 is an image of one of these devices. The buckles are obvious compared to Figure 6, and we speculate the darker appearance of the films in Figure 7 may be due to improved light harvesting. The device was formed by casting films directly on buckles. One of the issues we faced is making reliable electrical contacts, which we believe is due to the buckles. We describe the performance of buckled substrates and improvements of electrical contacts in Section 3.2.3.

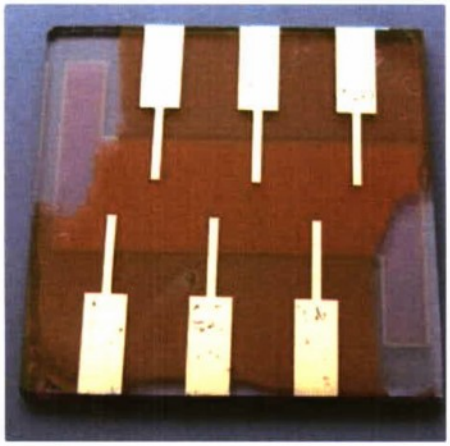

Figure 6. Photograph of prototype planar OPV devices based on active layer films with improved uniformity.

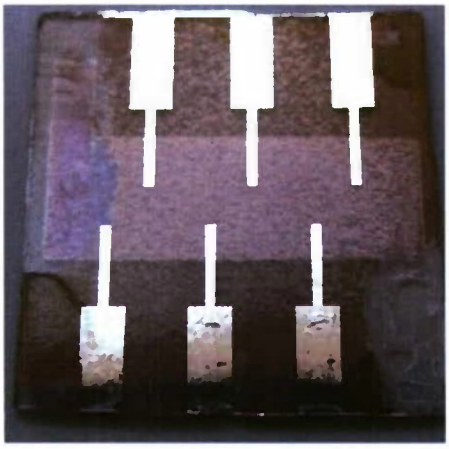

Figure 7. Photograph of prototype buckled OPV device. The devices were contacted on the corners (upper left and lower right), but did not produce reliable electrical contacts.

As mentioned previously, we developed a method to replica mold (i.e., transfer) buckled substrates into other materials such as thiol-enes and epoxies such that we can produce identical copies of the buckles rapidly. We compared the replication fidelity of several different materials. All of the materials replicated the buckles accurately based on the dimensions of the replicas relative to the master substrate. We also measured the glass transition temperatures of these materials, which is an important parameter for controlling mechanical stability during processing. In some cases, we want the substrates to maintain stability, whereas in others we would like to be able to induce buckling by raising the substrate temperature beyond the glass transition temperature.

We also established a quantitative way to characterize the buckles. One approach to characterizing the geometry of buckles is to make multiple measurements by profilometery or optical microscopy to determine the wavelength. This method is tedious and can lead to errors considering there is typically a distribution of wavelengths. We therefore explored fast Fourier analysis of our images. Figure 8 is a typical analysis.

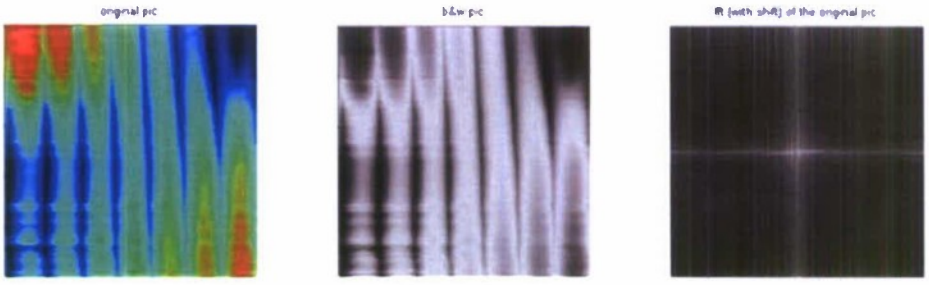

Figure 8. (left to right) Profilometry scan of oriented buckles (left) converted to black and white (center). (right) The FFT spectra of the buckles provides information about the characteristic wavelength in a more holistic manner.

To ensure we are interpreting the FFT spectra correctly, we inputted pictures with known geometries (for example, arrays of lines or circles) into the software we wrote and analyzed the output to create a baseline understanding. From that analysis, we used the FFT approach to characterize complex, hierarchical buckles, such as those shown in Figure 9. The image in Figure 9 contains multiple wavelengths (approximated to be 3-6 microns for the smaller wavelengths and ~20 microns for the larger wavelengths). Using our FFT method, we determined that the wavelengths to be ~4 and ~18 microns. The use of the FFT approach minimizes human bias in the measurements and provides characteristic wavelengths rather than the average of many measurements (i.e., it is more efficient).

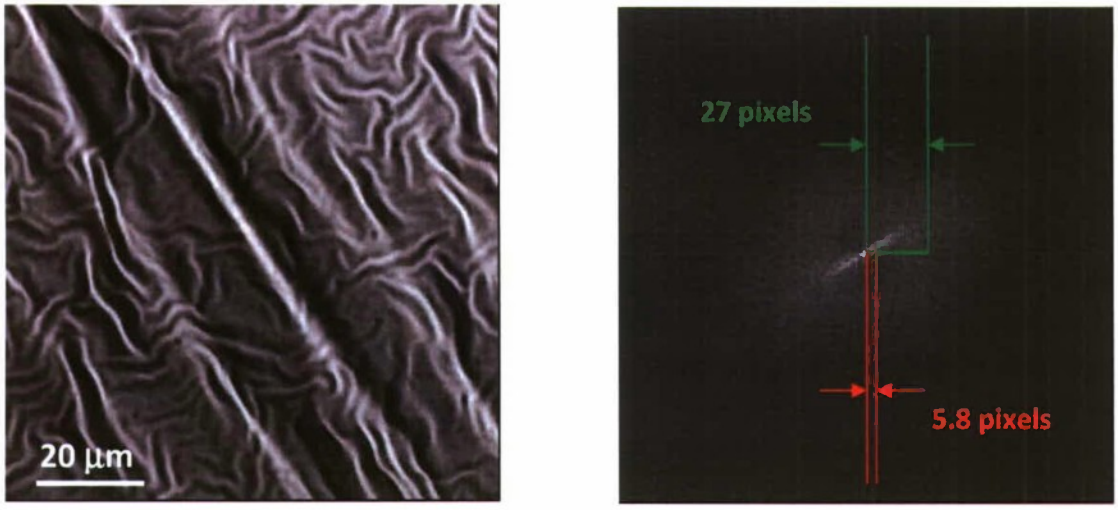

Figure 9. Demonstration of the utility of the 2D-FFT analysis of hierarchical buckles. Left – an optical micrograph of buckles with multiple wavelengths. Right – the FFT spectra of the image that gives two characteristic spacings for the two wavelengths apparent on the left.

3.1.3. Increasing the Aspect Ratio of Buckles

An inherent limitation of buckles is they adopt geometries with low aspect ratios (typically less than 0.2). Figure 10 is a cross-section scanning electron micrograph of PDMS buckles. The aspect ratio of this particularly sample is ~0.2 (amplitude to period). We assumed that the best devices would represent a trade-off between optimized light collection (presumably favored by high aspect ratios) and reliability (presumably favored by low aspect ratios, which present the least amount of film stack stress). We sought simple ways to increase the aspect ratios using stresses that could be easily applied externally. In hindsight, thermal buckles with low aspect ratios are sufficient to provide significant gains in performance. Regardless, we report some key results here regarding aspect ratio amplification for posterity and also because some of the processes are compatible with thermal buckles and could potentially provide additional gain in performance.

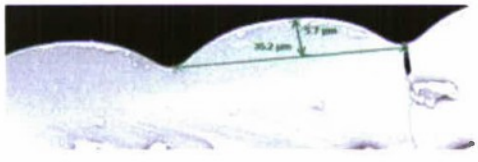

Figure 10. Cross sectional SEM image of a buckled substrate.

The use of electric fields to amplify the amplitude is a simple and therefore appealing approach. Figure 11 depicts the general idea. A thin film stack consisting of a conductor on top of a thin polymer film is deposited onto a conductive substrate. An electric field applied between the top and bottom films amplifies the buckles via electrostatic forces.

A primary benefit to this approach is that neither mechanical nor thermal stresses are required to produce the buckling effect, so it may be more compatible with a wider range of devices without producing negative effects. It is also appealing because it uses geometries that are already present in our PV design.

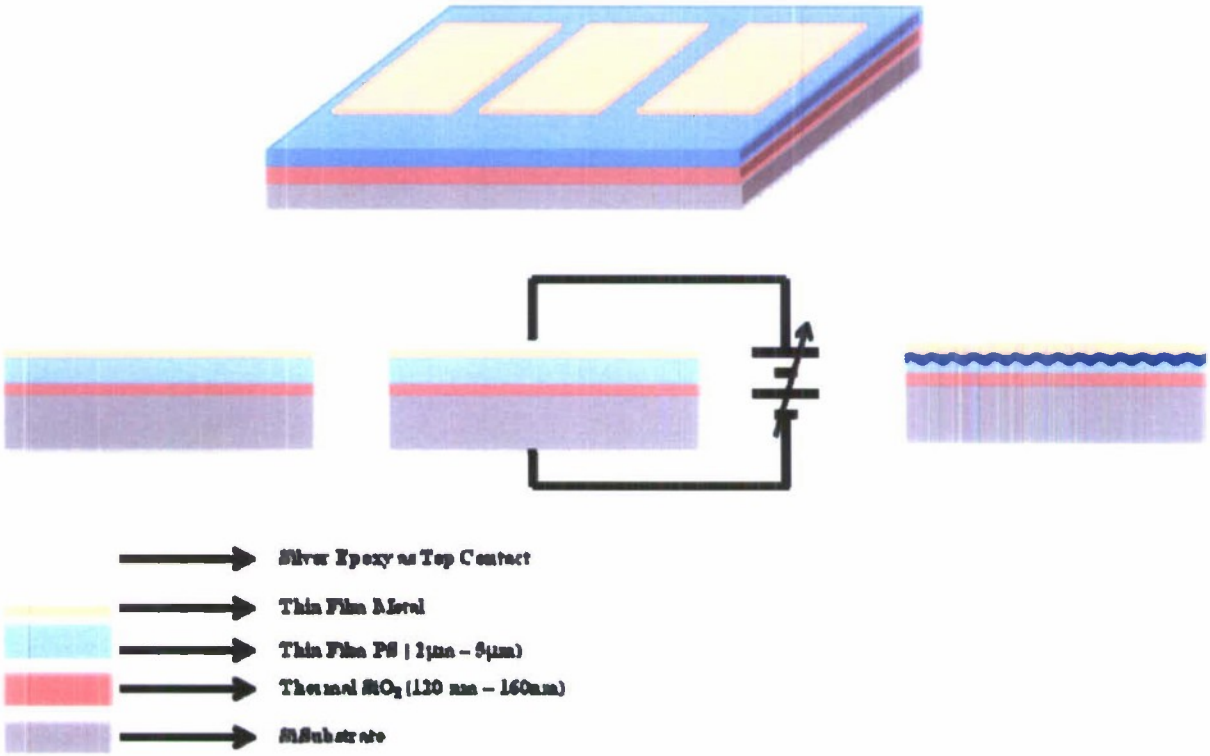

Figure 11. A pursued method to improve buckle aspect ratio. (Left) A thin film (orange) is deposited onto a thin film of polymer (e.g., polystyrene, depicted in blue) supported by a substrate (pink). (Middle) Applying a voltage across the blue film while heating the substrate will cause the buckles to amplify (Right).

We used an aluminum thin film supported by a polystyrene film as our model substrate. Figure 12 is a series of images of buckles with and without application of an electric field. The round shape in the bottom of the images is a silver paste electrode that is used to connect external electrodes to the film. It is apparent from Figure 12 that the electric field has a profound influence on the buckles. The amplitude increases by a factor of 3 relative to the control (i.e., no electric field). Unfortunately, the ultimate aspect ratio was still low (~0.1).

Figure 12. Micrographs of thermal buckles with (left) and without (right) an applied electric field. It is apparent that the electric field causes the buckles to change their morphology.

We also explored the use of solvent swelling to induce more stress in substrates, and thereby amplify buckles. Figure 13 shows the basic concept. An appeal of this approach is both its simplicity and the fact that some OPV processes use solvent (and therefore would require no additional steps).

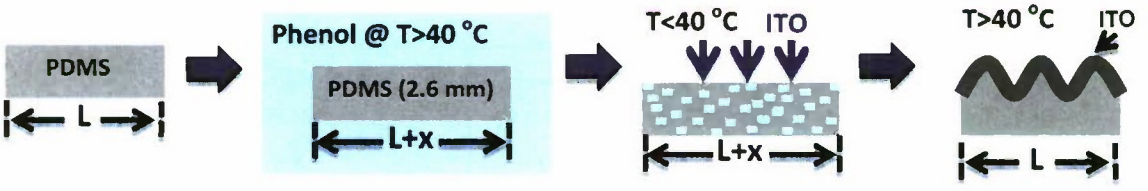

Figure 13. Another strategy for increasing aspect ratio of buckles. Swelling creates additional stress that can cause buckling.

A more immediately useful approach of solvent swelling is to harness it to induce buckling in thin films, such as Al. Figure 14 shows films of Al on polystyrene exposed to toluene vapor for 24 hours. The films buckle with large amplitude, but the aspect ratio is not any better than mechanical buckles (~0.1). We concluded that solvent swelling is interesting from an academic perspective, but would not be immediately helpful for the goals of this project.

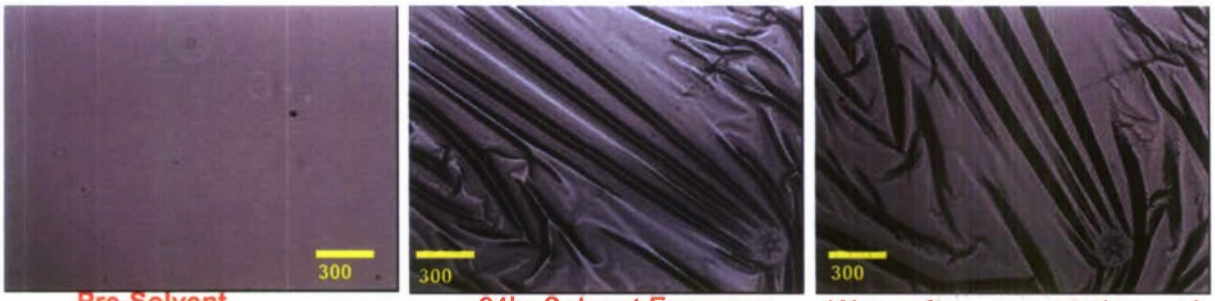

Figure 14. As thin films of polystyrene supporting thin aluminum films are exposed to solvent vapor, the polymer swells and creates stress that induces buckles.

3.2 Demonstrate improved light harvesting using small-molecule OPV devices

3.2.1 Highlights

- Fabricated small molecule OPV device on mechanically and thermally buckled substrates
- Resolved challenges associated with making electrical contact to buckle topology devices.
- Studied issues that lead to initially poor performance and low yield of buckled OPVs
- Identified and resolved problems with low fill factors and short circuits in devices made on in-house deposited ITO
- Repeatedly demonstrated buckled OPVs that show significant increase in current over their planar equivalent
- Increased buckled OPV device fill factor to 0.55. This fill factor compares well to the maximum fill factor for planar devices of 0.6 that we had previously observed.
- Demonstrated overall improvement in power conversion efficiency for buckled devices over their planar equivalent

3.2.2 Optical Characterization

We utilized a number of optical characterization techniques to evaluate the impact that different topography substrates could have on the electrical performance of photovoltaic devices. Optical characterization typically consisted of measuring the spectral absorption of a set of active layer materials (for example C_{60} and CuPC – two of the primary OPV absorber materials that were employed during this work) on both planar and scattering substrates (of various types). Optical characterization had the benefit of being a relatively rapid measurement process. It also focused on the substrate's impact on light absorption without interference from electronic defects that can influence electrical device measurements. That being said, we did find that optical characterization possessed its own shortcomings. Most notably were the limitations imposed by our instruments and the artifacts that they introduced into the measurements. As a consequence we spent a certain amount of time working on resolving these artifacts in order to increase our confidence on the measurement outcomes from the optical characterization.

At the project outset we performed a preliminary evaluation of the impact of thermally induced topography on optical absorption. We measured the spectral reflectance of two buckled topography samples and compared them to one planar sample. Because the metal layer was opaque, the inverse of the measured reflection is the absorption. We compared the results to the absorption of the same CuPc/C_{60}/Al stack deposited on a smooth glass substrate. The absorption spectra are shown in Figure 15. These data showed that the two topographies exhibited different absorption, but that both are substantially higher than the smooth sample. The cause of the gradual increase with increasing wavelength is not clear but the increased absorption centered around ~550 nm is due to CuPc absorption, which was a clear indication that the buckled topography could lead to increased optical absorption by the active PV layers.

We then examined the optical response of a complete OPV device stack (including the blocking layer BCP and the transparent conducting ITO contact. Figure 16 shows the reflection spectra (a lower reflectance implies improved absorption) of this photovoltaic film stack built on a planar substrate ("unbuckled"), on a pre-buckled substrate, and on a planar substrate that was subsequently buckled. It was observed that the post-deposition thermal buckles showed a marked decreased reflection but we were concerned that the baseline reflection in the infrared (e.g. in the 1000 to 1200 nm region) where there is nominally minimal absorption from the active materials was as high as it appeared. This caused us to question the measurement and led us to pursue optical measurements in both a simpler material system and to explore methods for mathematically modeling our system and measurements.

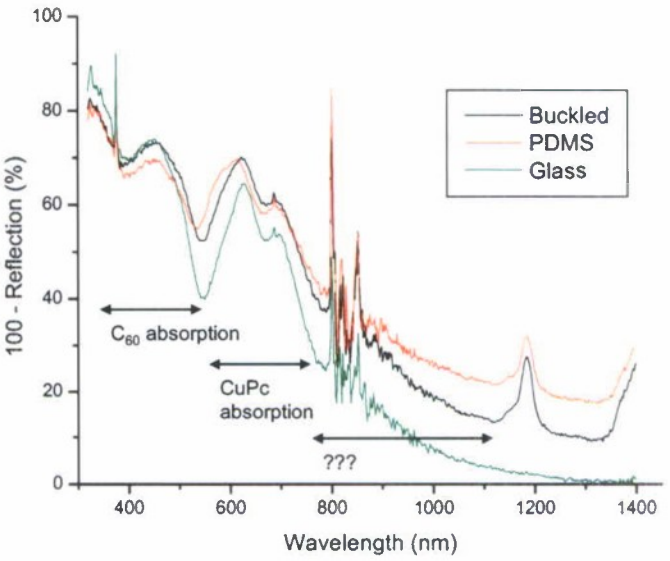

Figure 15. Absorption spectra for two buckled samples compared to a smooth glass substrate.

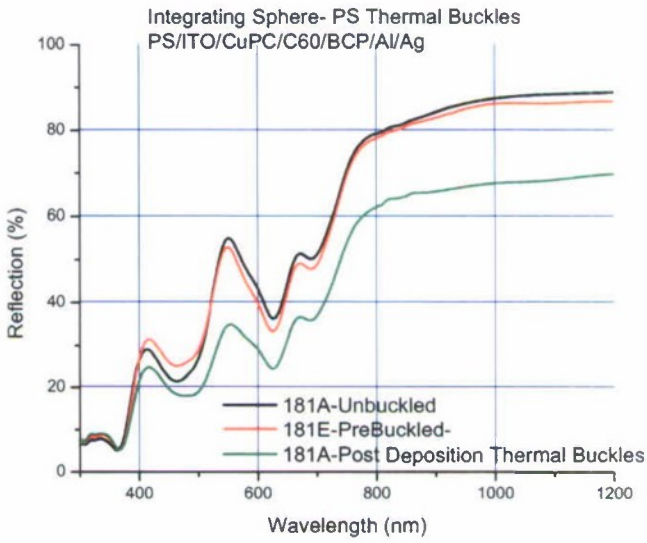

Figure 16. Reflection spectra showing that a buckled substrate (green) is less reflective than a planar substrate (black). Light which is not reflected has been absorbed by the device. The film stack in these measurements is identical to that used in small molecule OPV devices.

We initially performed optical measurements using a UV-Vis spectrometer in RTI's facilities. As the project progressed we began working in parallel with a new system at NCSU. We also started working to interpret our measurements with mathematical modeling. We identified a ray tracing software called "TracePro" that was available at NC State and a student learned how to use it so we could better understand our experimental measurements.

Further work with quantifying the effects of topography on optical absorption occurred using the absorption spectrometer and integrating sphere at NCSU. We produced a matrix of model substrates to evaluate the improvements in absorption realized by different methods of buckling. Figure 17 shows a representative result from this work.

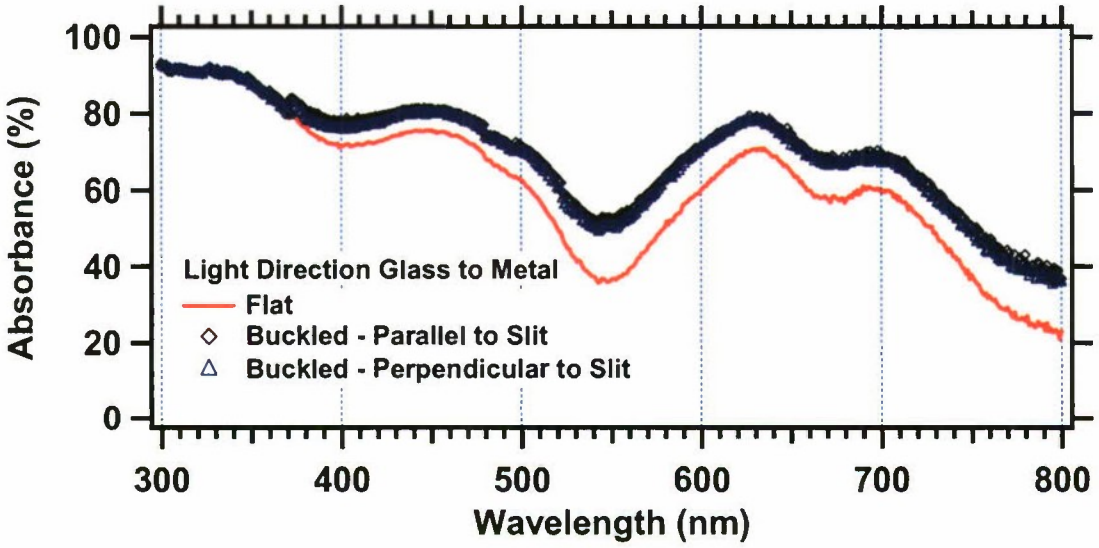

Figure 17. An absorbance spectra of a buckled OPV versus a planar OPV. The buckled OPV shows increased absorbance, which is desirable.

As we performed this work we also continued to try to elucidate some complexities with the integrating sphere. For example, consider the results of Figure 18, in which we measured the reflection spectra of a simple metal film that is flat versus one that is buckled (with the buckles oriented at two different configurations relative to the slit of the integrating sphere). In principle, both substrates should reflect similarly since there is nothing to absorb the light, but according to the measurement, the buckled sample reflects more than the flat sample. Furthermore, the mirror should reflect no more than 100%, but these measurements (which were been repeated several times) exceeded 100%.

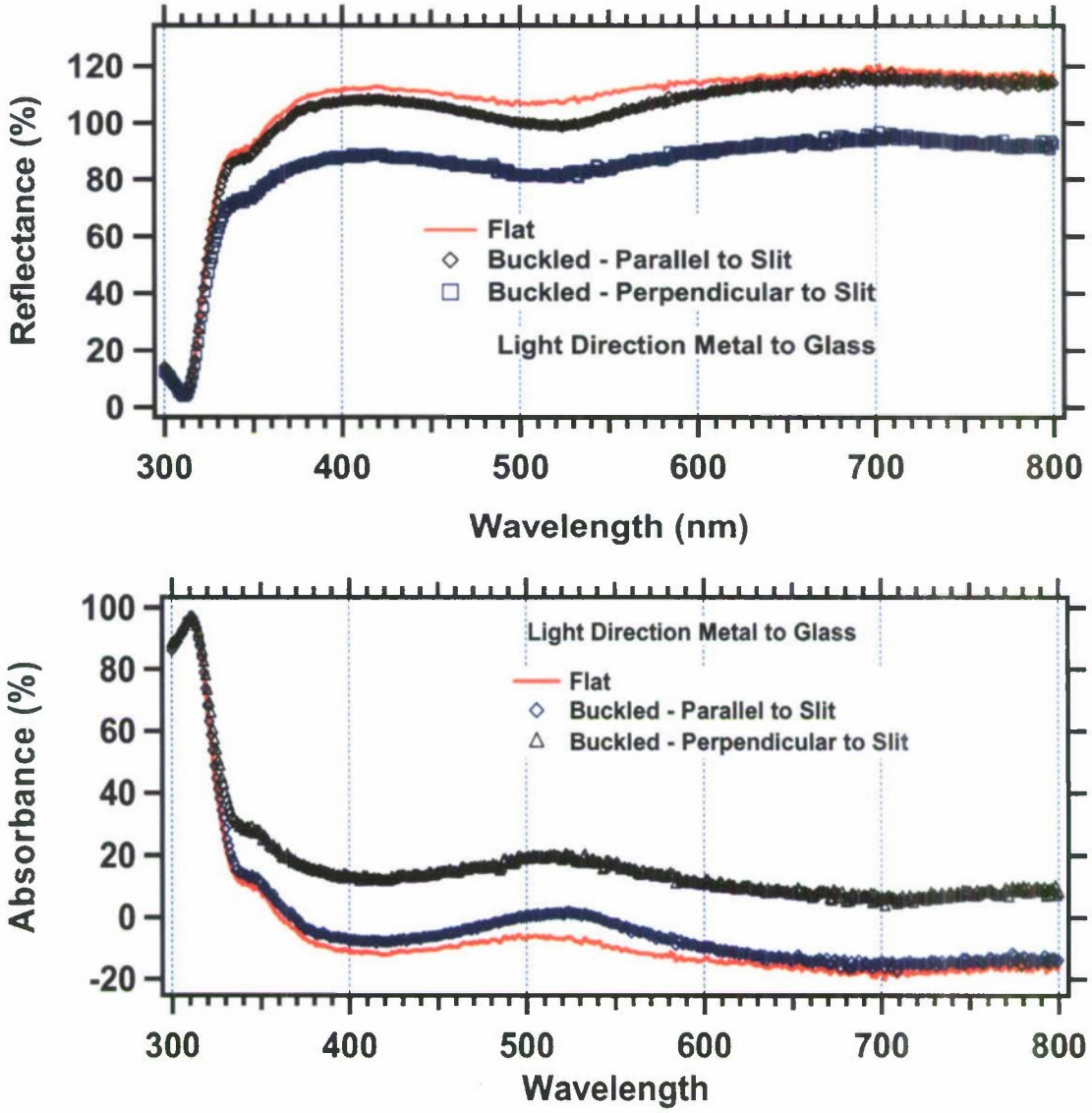

Figure 18. An absorbance and reflection spectra of a buckled metal film versus a flat metal film. These results indicate some of the challenges associated with the interpretation of our other integrating sphere measurements (i.e., actual OPV devices).

In addition to creating "thermal" buckles with various wavelengths, we replicated the anti-reflective texture on Si solar cells as a basis for comparison. The texture on these cells has higher aspect ratios (~0.3) than the thermal buckles. Figure 19 shows the textured Si topography. We created both positive and inverse (negative) replicas of the topography, as shown in Figure 20.

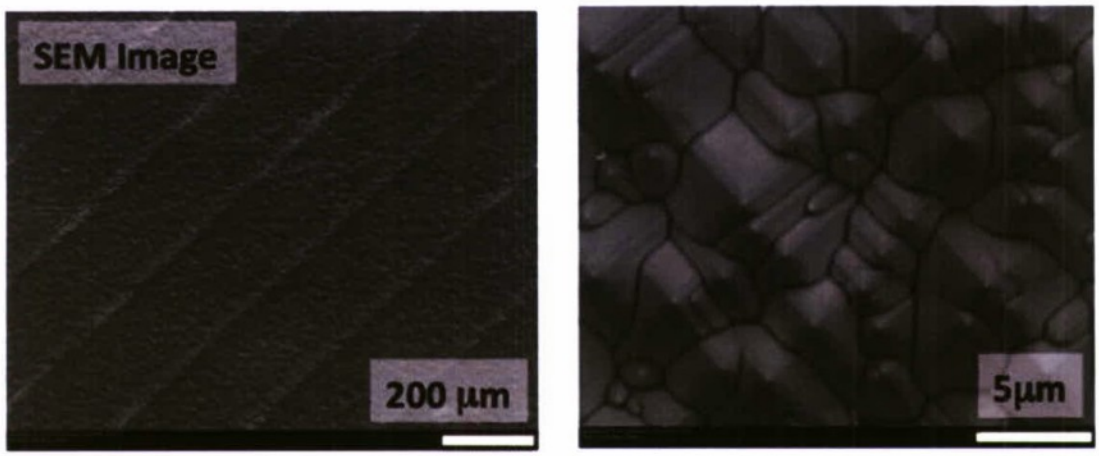

Figure 19. Scanning electron micrographs of the surface of model textured Si solar cells.

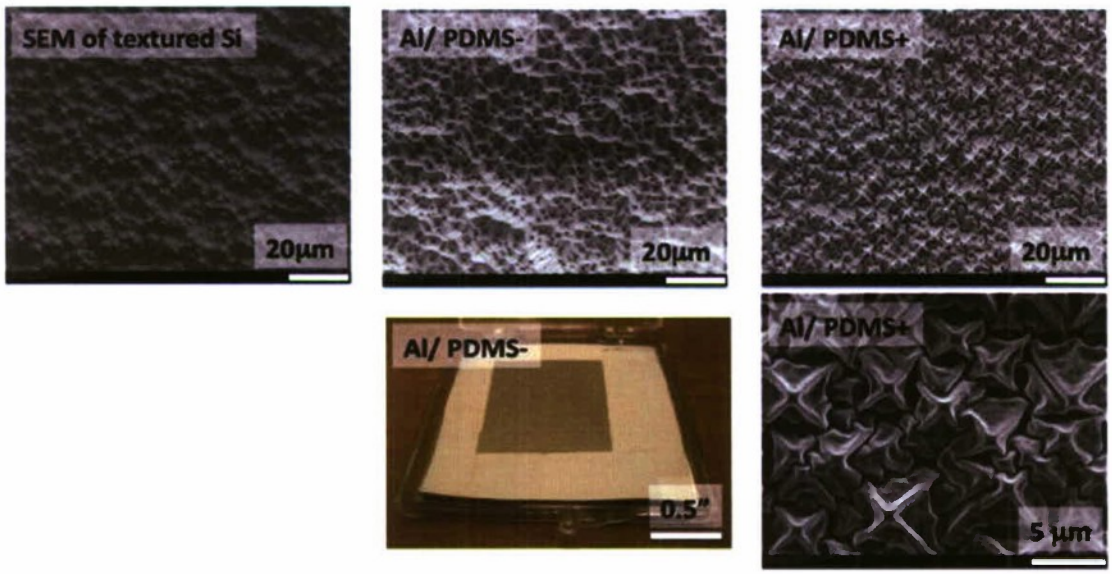

Figure 20. Images of the textured Si and the PDMS replicas (both positive and negative).

Onto these buckled surfaces we deposited the OPV optical absorber (C_{60}/CuPC) materials and measured the absorbance using a UV-Vis equipped with the integrating sphere. Figure 21 shows the results that compared these substrates. The thermal buckled substrates (which have smaller aspect ratios compared with mechanical buckles) showed modest improvements over planar devices. The Si texture, however,

showed a significant improvement in absorption. These results suggested that larger aspect ratios are required in order to obtain large enhancements in optical absorption.

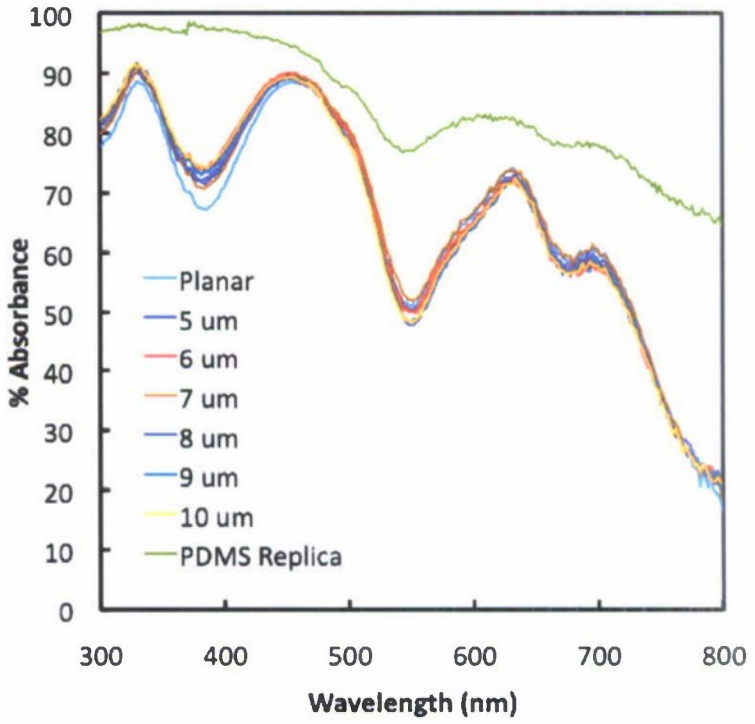

Figure 21. UV-Vis absorbance data that shows how high-aspect ratio topography has a larger impact on improving optical absorption than low-aspect ratio topography.

We continued to interpret our optical data with a skeptical eye as we tried to elucidate some complexities with the integrating sphere. We made measurements that showed mirrors that reflected more than 100%, but these measurements did not make sense physically. We worked to separate instrument artifacts from real effects by comparing the integrating spheres between RTI and NCSU, and working with the manufacturer of the integrating sphere. We also created a working model of an integrating sphere in a ray tracing software called "TracePro". Figure 22 is a screen shot of our model that shows the inner workings of the sphere. Figure 23 shows that a mirrored sample could have greater than 100% based on this simple model. We then consulted with world leaders on integrating spheres (both at Thermo Electron and Lab Sphere) and nobody understood these results. Apparently this result has not been observed previously by the manufacturers of the sphere.

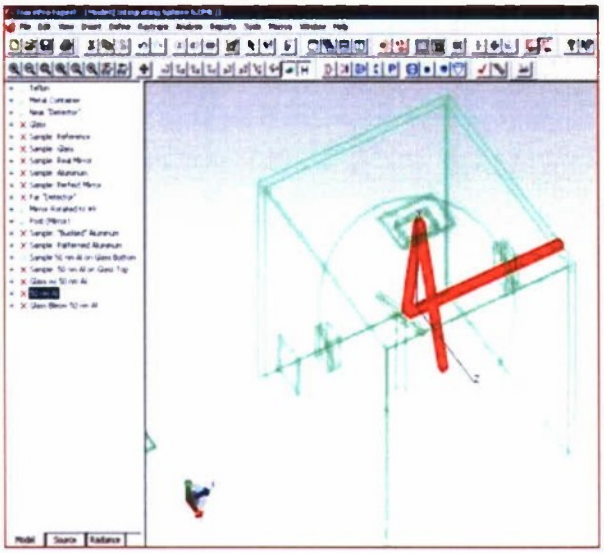

Figure 22. A screen shot from TracePro of an integrating sphere model we developed to better understand the data from the integrating sphere.

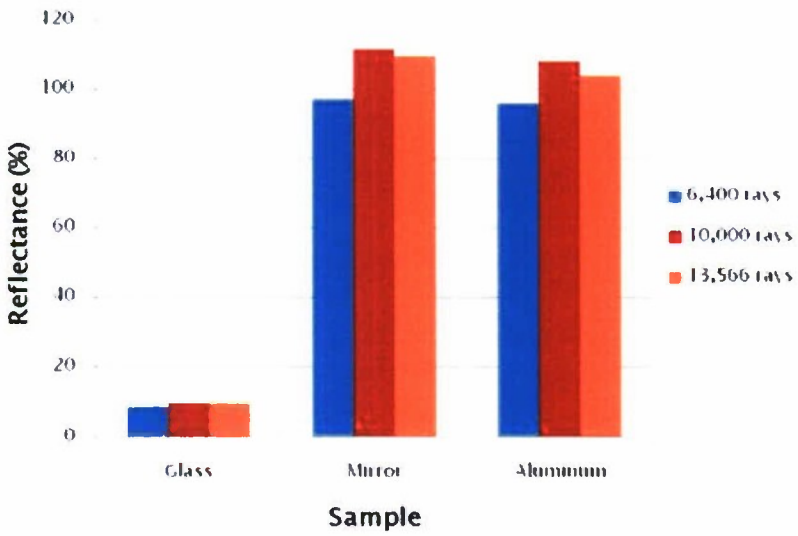

Figure 23. Initial data from the integrating sphere model confirms that some mirrors give >100% reflectance, which is surprising. The answer depends on the number of rays because of the stochastic nature of the software.

Nonetheless we pressed on with our measurements, refining our measurement techniques. One such refinement can be seen in the use of a buckled mirror for a reference instead of a flat diffuse reflector. Using this refinement we measured the

optical absorption properties of "thermal" buckles (with various wavelengths) and replicated Si topography buckles. These results can be seen in Figure 24.

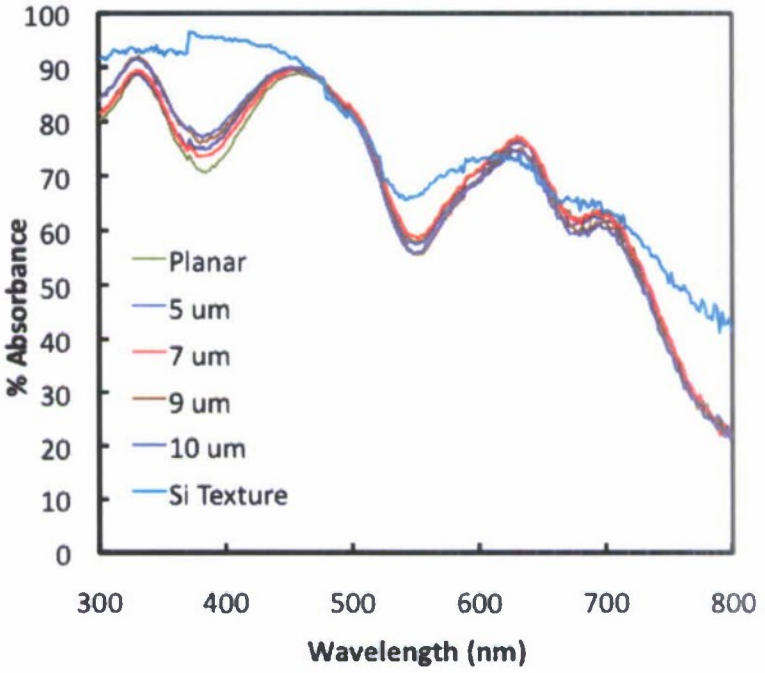

Figure 24. UV-Vis absorbance data that shows how high-aspect ratio topography has a larger impact on improving optical absorption than low-aspect ratio topography.

These measurements, like those shown earlier, confirmed that low aspect ratio topography has a small improvement on absorption but that high aspect ratio topography can lead to a more dramatic increase in light harvesting.

3.2.3 Electrical Characterization

Complete OPV test devices were fabricated throughout the project. These devices were meant to establish baseline performance of planar devices and to test the impact that the various high topography substrates had on photovoltaic performance. The primary measurement technique used to characterize these devices was the current-voltage curve (I-V), taken without illumination (dark) and with simulated solar illumination (light). During a typical device test two test leads are connect to the solar cell and the voltage is scanned while the current response is measured. This is done both in the dark and in the light. From this measurement, four device performance parameters are extracted. The first of these is power conversion efficiency (PCE), which is the ratio of the incident optical power to the extracted electrical power. The second is short circuit current (ISC), which is the maximum possible photogenerated current that can be extracted from the

device. The third is the open circuit voltage (VOC), which is the maximum voltage that is developed across the device terminals during solar illumination. The fourth is the fill factor (FF) which is a figure of merit that describes how close to an ideal, lossless diode the PV device is. A reduced FF has the impact of reducing the maximum power output of a device.

To establish baseline PV device performance we fabricated a number of OPV devices using organic small molecules. These devices were composed of the following device stack: Glass/ITO/CuPc/C_{60}/BCP/Al/Ag. We initially fabricated devices on commercial glass slides coated with ITO. Preliminary devices tested under illumination from a solar simulator (AM1.5G spectrum with 100 mW/cm^2 optical power density) showed a power conversion efficiency of about 1.6%. This value compared favorably with that reported by other research groups; of the many literature reports we have found only two groups report a higher efficiency. A representative current voltage plot showing a PV device in operation in the dark and under illumination can be seen in Figure 25.

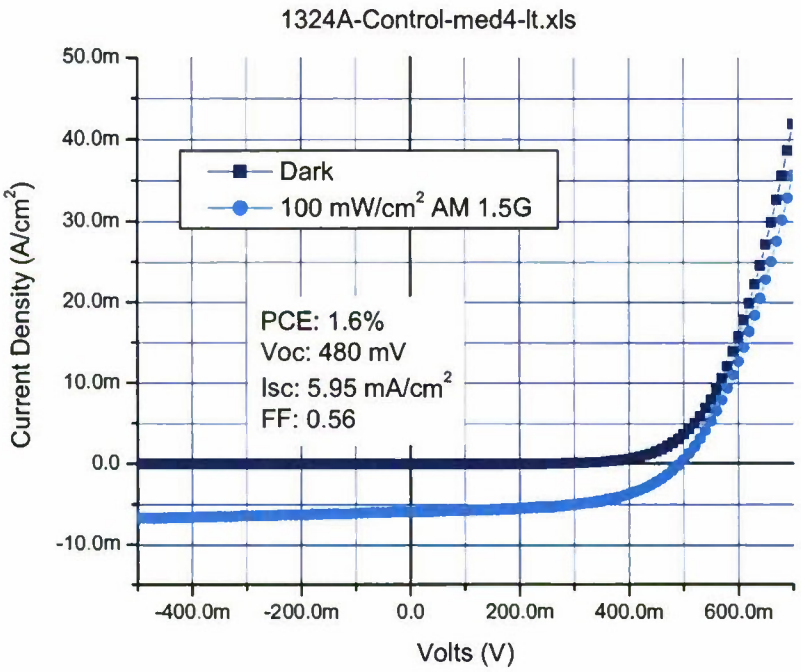

Figure 25. Current-voltage curves of OPV device on a commercial glass substrate showing operation in the dark and under optical illumination.

Our first attempt to fabricate an OPV device using a buckled substrate used a substrate fabricated via thermally induced buckling by depositing a layer of ITO onto a polystyrene (PS) layer, which was then heated to induce buckling. While the devices we fabricated

did show a photovoltaic effect, the buckled and planar devices made with in-house ITO exhibited reduced performance as compared to the control device made on commercial ITO. This performance reduction was almost entirely due to a reduced fill factor in these devices. This observation led us to hypothesize that the devices suffered from high series resistance as compared to the device fabricated on commercial ITO. While we initially thought that the series resistance was due to differences in the resistivity between the in-house ITO and the commercially purchased ITO (and performed some experiments to examine this), we found that contact problems primarily contributed to the poor FF. The standard method of making contact to the ITO layer was damaging the film due to the softer PS layer underneath, resulting in high and unrepeatable contact resistance. To overcome this problem set out to investigate a number of alternate contacting strategies.

The transparent contact in our PV device stack is a ~120 nm thick film of ITO (indium tin oxide) which is deposited onto a device substrate at NCSU. The majority of research on next generation PV technologies is done using commercially purchased glass substrates which come pre-coated with ITO. As this project was focused on building devices using buckled substrates we are required to deposit our ITO in-house. ITO deposition is not necessarily a high risk process but nonetheless it plays an important role in device performance. As such we sought to evaluate the quality of our ITO by fabricating OPV devices on both planar commercially prepared ITO and planar NCSU prepared ITO. Table 2 summarizes the results of this experiment. In it one can see that the average device performance of the NCSU-ITO device was higher than that of the commercial ITO.

To overcome the contact problems that we had initially attributed our poor high topography device results we investigated the use of adhering conductive copper tape to the sample. Instead of contacting directly to the buckled ITO we landed our probe tip onto the copper tape. We then fabricated and tested a new set of buckled substrate devices. In the same device run we also fabricated a planar equivalent and compared the performance of the devices. Table 3 summarizes the findings of this experiment.

The primary finding of this experiment was that the use of the buckled substrate did not improve device performance over that of the planar equivalent. Looking at the average performance numbers one can see that the planar device had a higher average fill factor and a higher average short circuit current. These two differences resulted in a higher average power conversion efficiency. The Is of a PV device arises from a multi-step process. The first step is the absorption of incident light. It is this step we seek to enhance by using buckled topology substrates. Other steps in the process include charge separation and charge extraction. These steps are largely determined by a material's electronic properties.

Table 2. Performance summary comparing devices fabricated on commercially prepared ITO and ITO prepared at NCSU.

Device	Description	PCE (%)	VOC (V)	ISC (mA/cm^2)	FF
1334D-1	Commercial ITO on glass	1.31	0.44	4.92	0.607
1334D-2	Commercial ITO on glass	1.4	0.45	5.19	0.599
1334D-3	Commercial ITO on glass	1.36	0.44	5.01	0.617
Average		**1.36**	**0.44**	**5.04**	**0.61**
1334B-1	NCSU ITO on Glass	1.55	0.45	5.78	0.597
1334B-2	NCSU ITO on Glass	1.49	0.45	5.71	0.580
1334B-3	NCSU ITO on Glass	1.52	0.45	5.66	0.599
1334B-4	NCSU ITO on Glass	1.55	0.45	5.79	0.595
Average		**1.53**	**0.45**	**5.74**	**0.592**

Table 3 Performance summary comparing devices fabricated on commercially prepared ITO and ITO prepared at NCSU.

Device	Description	PCE (%)	VOC (V)	ISC (mA/cm^2)	FF
1334C-1	Planar-PS-ITO	1.43	0.45	5.25	0.604
1334C-2	Planar-PS-ITO	1.53	0.45	5.53	0.615
1334C-3	Planar-PS-ITO	1.52	0.45	5.51	0.615
1334C-4	Planar-PS-ITO	1.4	0.45	5.22	0.596
Average		**1.47**	**0.45**	**5.38**	**0.608**
1326B-1	Buckled-PS- ITO	1.24	0.47	4.78	0.551
1326B-2	Buckled-PS- ITO	1.31	0.46	5.13	0.557
1326B-3	Buckled-PS- ITO	1.18	0.44	4.62	0.579
1326B-4	Buckled-PS- ITO	1.33	0.45	5.25	0.564
Average		**1.27**	**0.46**	**4.95**	**0.563**

Additional OPV devices were fabricated on mechanically-buckled substrates. We found that testing the devices proved problematic due to difficulties we had making good electrical contact to the top metal contact. Contacting problems resulted in artificially low fill factors (thanks to high series resistance) and reduced short circuit current densities. Contact problems were not limited to the mechanically buckled samples but were also present when testing additional devices fabricated using substrates based upon thermally induced buckles. Testing devices fabricated on planar control substrates did not result in the same problems.

We hypothesized that the cause of the contacting problems was likely tied to the device architecture and the method of probing the devices during test. The small molecule OPV devices are fabricated using a sandwich structure. The top metal contact is deposited as the last step in the fabrication process and forms a circle of metal which then defines the active area of the devices. To test each device a metal probe is lowered onto the circular metal contact. In planar devices we found that generally the best contact is made by pushing the probe very slightly across the surface of the metal contact. This was thought to break through the thin oxide barrier on the surface of the contact. While this method generally works well for planar devices, on buckled topography devices when the probe slides across the contact surface it immediately hits a buckle feature and gouges through it. This ends up damaging the device.

We tried a number of different methods to overcome this problem. These included: 1) changing probe materials (Au and In were tried) to use softer metals, 2) using very thin whisker probes, 3) using Ag paint and thin copper wires to make hand-made wire bonds, and 4) using a eutectic InGa metal which is liquid at room temperature. None of these produced satisfactory results.

Our next step was to develop a device architecture that did not rely on landing a probe on the top contact. Instead we produced devices where both the top and the bottom contact are patterned to form a "cross-bar" design. In a cross-bar design the top and bottom contacts (ITO and Al/Ag – in this case) run across the substrate at right angles to each other. The area where they overlap is the active area of the device. To test a device contact is made in regions where they don't overlap. This eliminates any possibility of accidentally punching through a contact and short-circuiting (or otherwise damaging) a device. To implement this device structure we designed and fabricating the masks we needed to pattern the contacts.

A graphic depicting the cross-bar design can be seen in Figure 26. The geometry may appear complicated because various layers are overlaid, but the general intent of the design was to move the electrical contacts to the perimeter of the substrate to facilitate electrical connections, while minimizing series resistance and eliminating problems with punching through the metal.

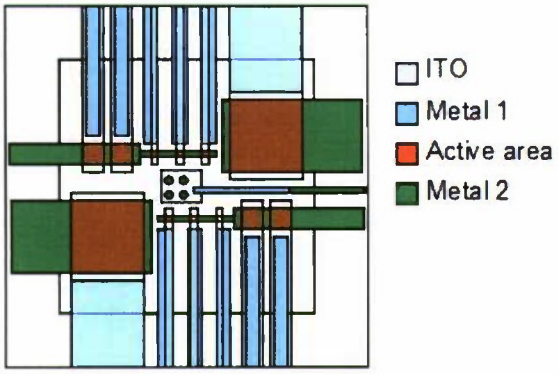

Figure 26. Graphic depicting the Cross Bar device design.

The design incorporates four different device geometries with areas that scale from 1 x 1 mm devices to 1 x 1 cm devices, as well as 1 mm diameter circular devices. The first step in the design fabrication is to produce patterned ITO (depicting in grey in Figure 26) on a blank 50 mm x 50 mm substrate. We accomplished this by photolithographically patterning a blanket layer of ITO or sputtering ITO through a shadow mask onto a blank substrate. The next step was to deposit metal layer 1 (depicting in blue in Figure 26). This layer serves to reduce the series resistance of the ITO stripes, improving device performance. Onto this we deposited the active material of the PV device. Finally the top metal contacts (depicted in green in Figure 26) are deposited. This completes the device stack. The active region of each individual device is depicted in brown in Figure 26 and corresponds to the region where the ITO and the OLED metal overlap.

To test this design we produced photomasks for patterning the ITO and shadow masks for depositing metal. We initially sought to compare the performance of PV devices fabricated using this new design with those fabricated using our standard circular top contacts. To accomplish this we made QDPV devices using both structures and compared their results. This comparison can be seen in Table 4. Examining the performance of these two sets of devices shows that the Cross Bar based devices perform at approximately the same level as the traditional circular (non cross-bar) devices.

Once we completed the evaluation of the new cross-bar device structure we applied it to fabricating OPV devices on high topography substrates. It was then that we observed for the first time a thermally buckled substrate with higher short circuit current densities than its planar equivalent. Data showing this result can be seen in Figure 27. Unfortunately the overall device performance (power conversion efficiency) was lower for all devices fabricated using ITO that was deposited and patterned at NCSU. Normally this would be a cause for significant skepticism of this result. However Figure 27 also shows that the short circuit current, which is the parameter most directly

influenced by absorption, was higher for the buckled substrate than for the control device with high efficiency.

Table 4. A comparison of QD Devices fabricated using our traditional "Dots" based architecture and the cross bar architecture.

Variation	PCE (%)	VOC (V)	ISC (mA/cm^2)	FF
Exch5210-std-Dots-Dev1	2.53	0.31	13.3	0.612
Exch5210-std-Dots-Dev2	2.52	0.31	12.9	0.63
Exch5210-std-Dots-Dev3	2.08	0.32	11.2	0.58
Exch5210-std-Dots-Dev4	2.47	0.31	12.5	0.64
Average	**2.404**	**0.312**	**12.4**	**0.622**
Exch5210-std-CrossBar-Dev1	2.46	0.31	12.7	0.625
Exch5210-std-CrossBar-Dev1	2.43	0.32	12.5	0.607
Exch5210-std-CrossBar-Dev1	2.18	0.31	11.5	0.61
Exch5210-std-CrossBar-Dev1	2.26	0.32	11.6	0.61
Average	**2.33**	**0.315**	**12.07**	**0.613**

As we continued to build of off this result we were finding that subsequent device fabrication runs showed problems with short-circuits or very poor fill factors; notably those fabricated on substrates which incorporated NCSU-deposited ITO. A set of device curves showing typical performance can be seen in Figure 28 and Figure 29, and demonstrate the difference in fill factor between the NCSU ITO device and the commercial ITO device.

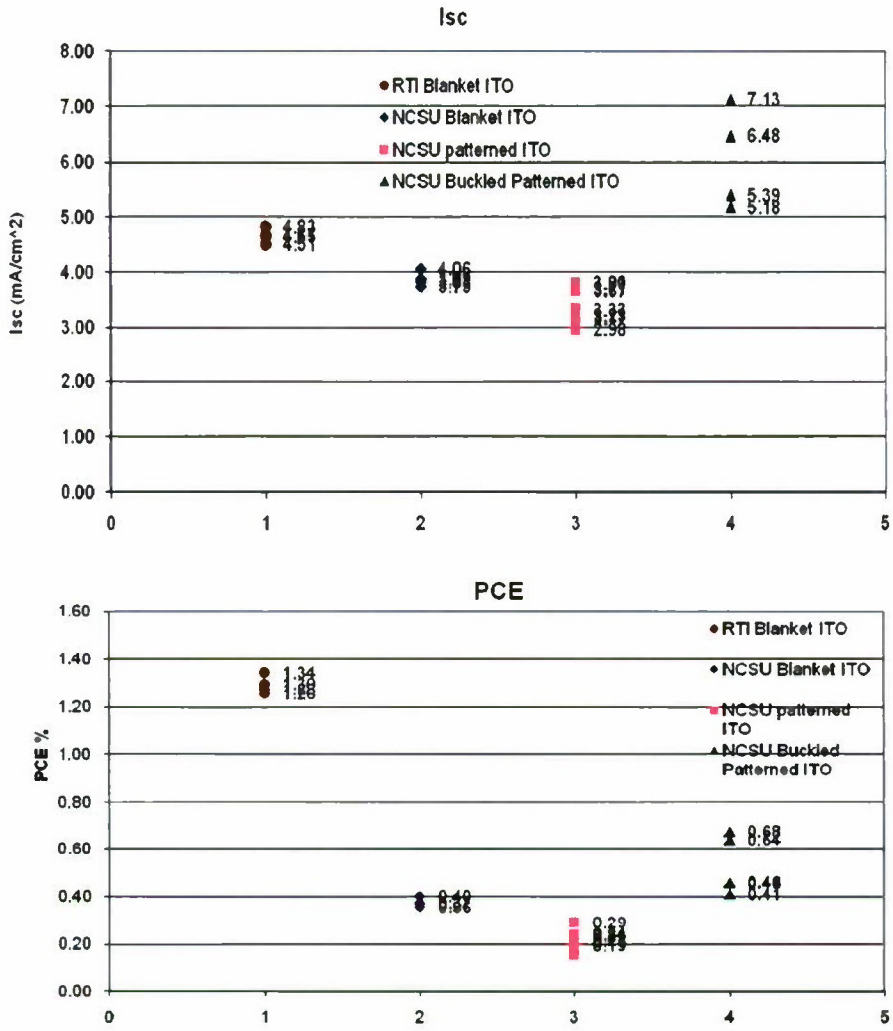

Figure 27. Chart showing the short circuit currents and power conversion efficiencies measured for a suite of PV devices fabricated on different substrate types. The data shows that the devices fabricated on the buckled ITO substrate had a higher short circuit current than the planar devices fabricated during the same device run.

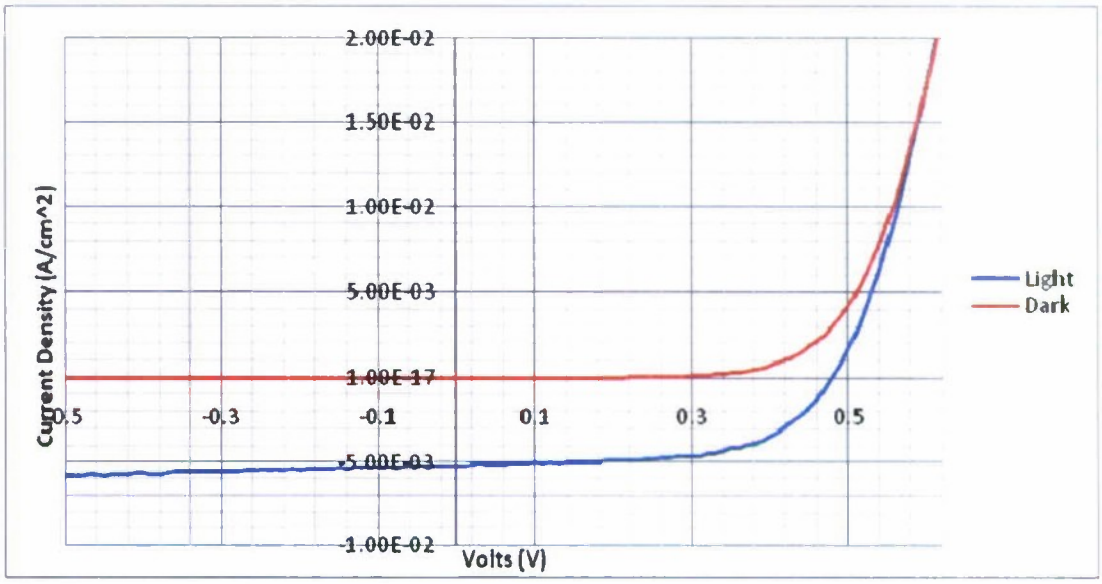

Figure 28. Light and dark current-voltage curves of a small molecule PV device fabricated on commercial ITO. The curves show good diode behaviour with a good fill factor (0.59).

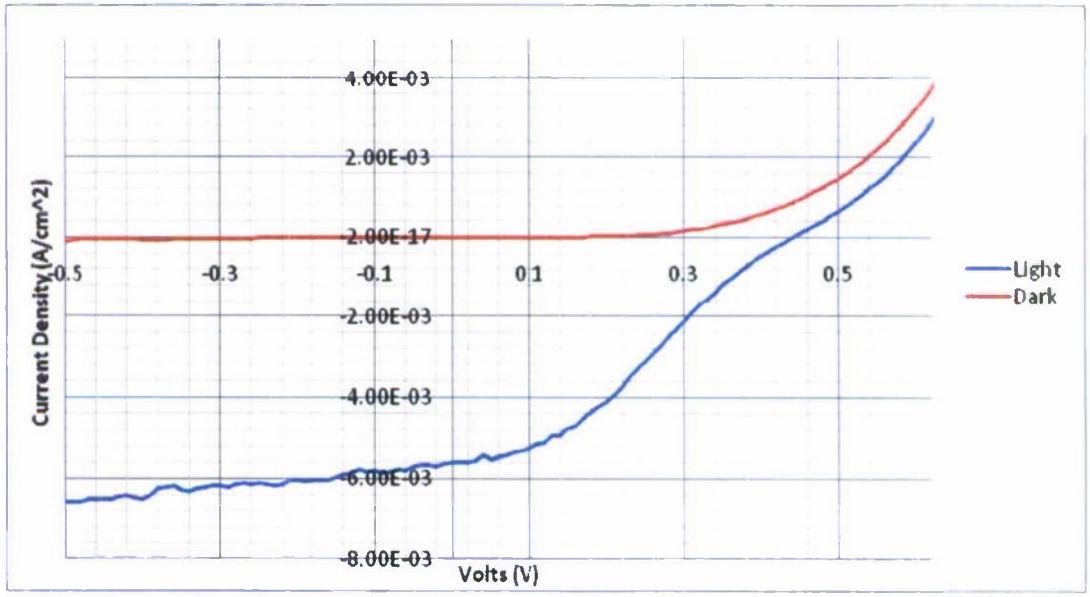

Figure 29. Light and dark current-voltage curves of a small molecule PV device fabricated on NCSU ITO. The curves show poor diode behaviour with a low fill factor (0.37).

A number of theories were proposed to explain the fill factor and shorting problems which we then tested and refined. The result of these efforts was the conclusion that device performance suffered from two problems. The first was an excess of small particles that were not being removed from the substrates after the ITO was deposited and before the CuPC/C60/BCP/Al layers were deposited. These particles contributed to the short circuit problem. Once we properly cleaned the substrates with an isopropanol/DI water rinse after ITO deposition we were able to solve our device shorting problem. The second problem arose as a result of a new procedure that was developed to pattern the ITO using photolithography. While this process resulted in ITO with clean edges (as opposed to the ITO deposited through a shadow mask), it appears to have left a residual organic layer (likely residual photoresist) that caused the fill factor to degrade and reduced device performance. To remove this residual layer we ran the patterned NCSU ITO substrates through a rigorous cleaning process. Devices fabricated on these cleaned substrates had performance on par with devices fabricated on commercial ITO and on unpatterned NCSU ITO. Data showing these results can be seen in Figure 30.

After observing the first indication that thermally buckled PS substrates increases the short circuit current of OPV devices we worked to both repeat the result and to increase the buckled device's power conversion performance. The primary reason that the buckled devices had demonstrated lower power conversion efficiency than their planar equivalent was due to a lower fill factor. We first showed a significant improvement in fill factor by improving the procedure for substrate cleaning, but found that this was still not sufficient. We then explored a number of cleaning techniques which included solvent rinsing, sonication and scrubbing, as well as oxygen/argon plasma cleaning. One of the solvent cleaning techniques led to a set of device whose PV performance is shown in Figure 31. In these devices one can see that the buckled PS devices once again showed higher short circuit current than their planar equivalent cross bar devices. The power conversion was still slightly lower due to a reduced fill factor, but showed improvement compared to previously reported results and provided the best result to date in that the overall power conversion efficiency was nearly as high for the buckled device as for the planar control.

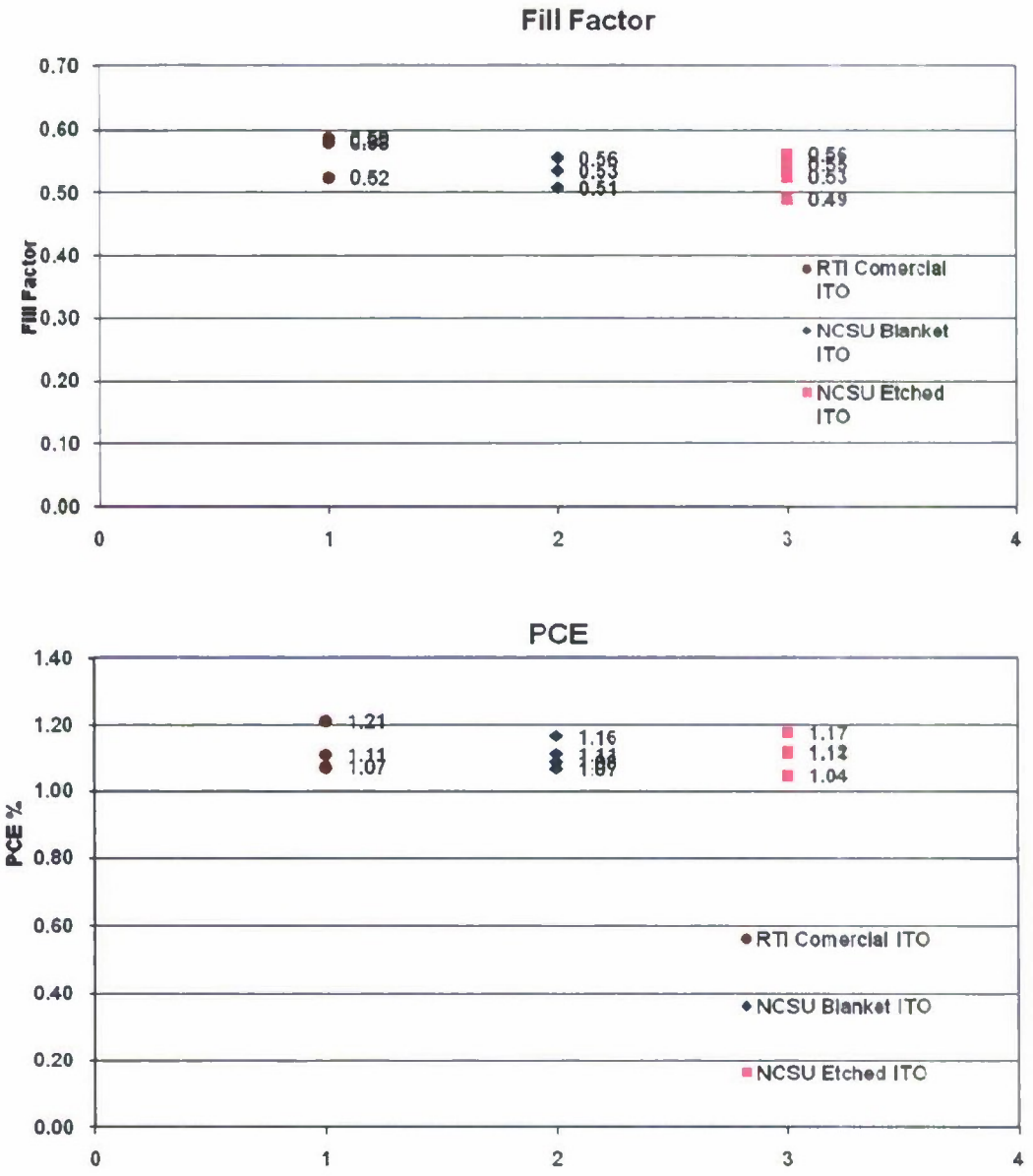

Figure 30. Chart showing the fill factors measured for a suite of PV devices fabricated on commercial ITO and NCSU ITO which were cleaned with a new procedure designed to remove residual organic material and particles. The data shows that the devices fabricated on the NCSU ITO had a very similar fill factor to those fabricated on the commerical ITO.

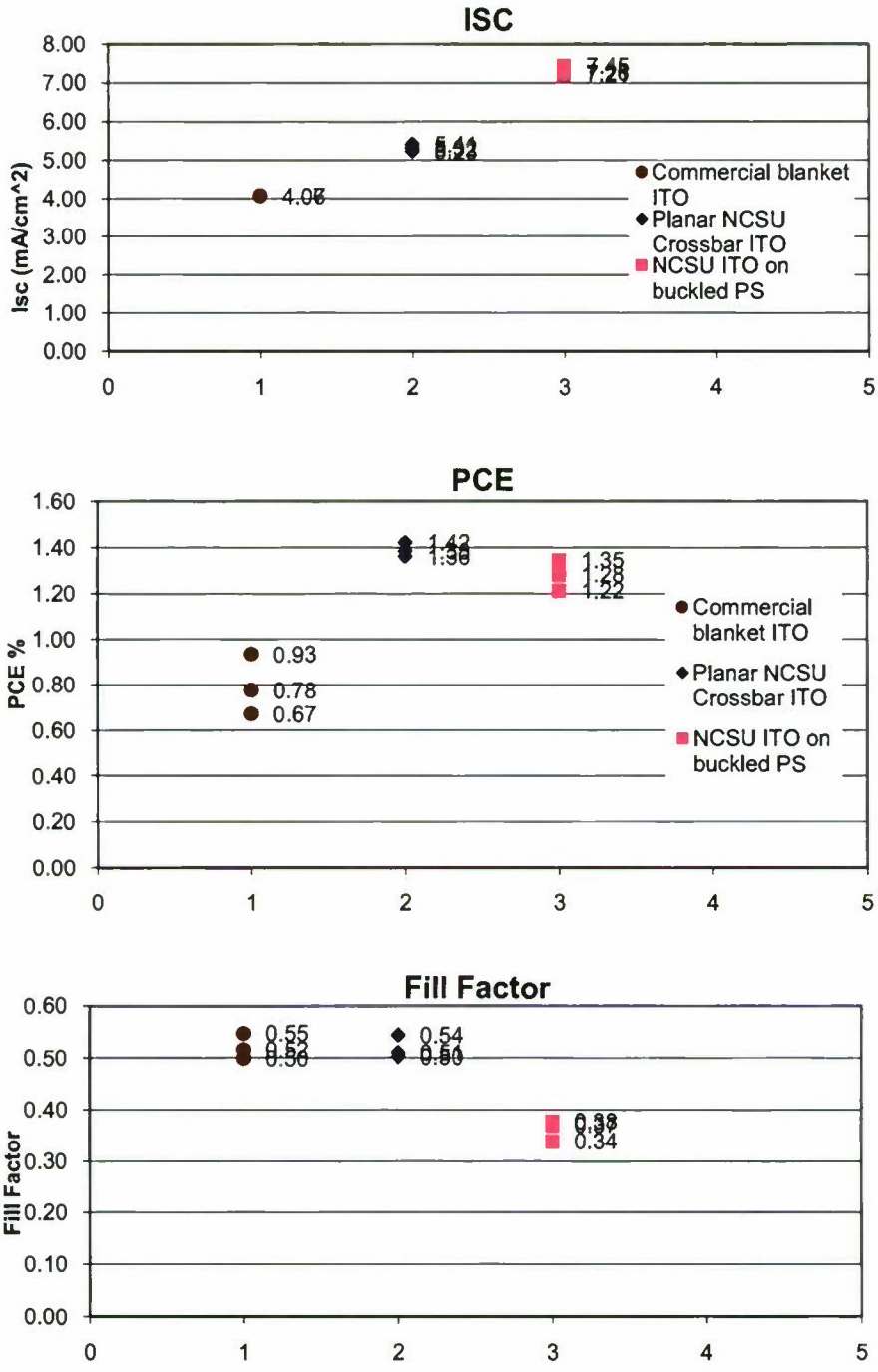

Figure 31. Chart showing the short circuit currents, power conversion efficiencies, and fill factors measured for a suite of PV devices fabricated on different substrate types. The data shows that the devices fabricated on the buckled ITO substrate had a higher short circuit current than the planar devices fabricated during the same device run.

To further improve the buckled OPV device's fill factors we examined the impact that an ultraviolet ozone (UVO) clean would have on device performance. UVO is similar to an oxygen plasma clean in that it is expected to remove organic contaminants from a substrate's surface but should do so in a gentler manner then plasma. A chart summarizing the results of these experiments can be seen in Figure 32.

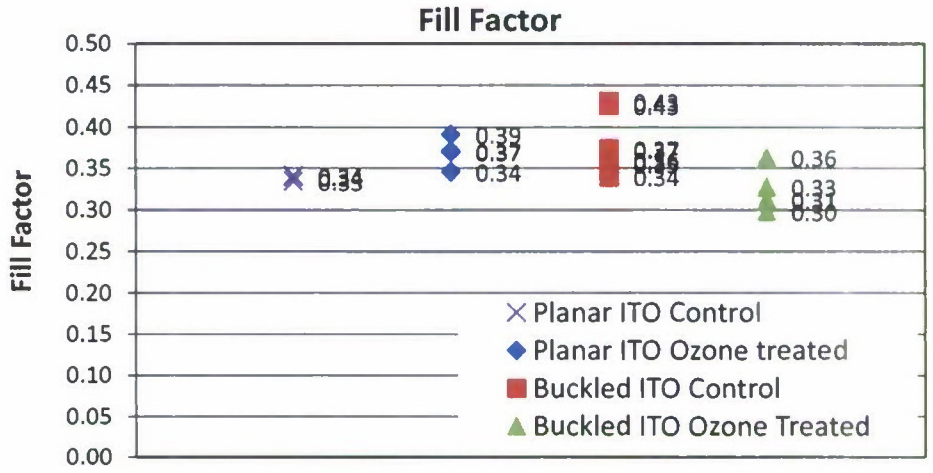

Figure 32. Results of experiments examining the impact of UV Ozone treatment on the fill factor of OPV devices.

One can see that the ozone treatment did not have a significant impact on the device fill factor. In fact when it was applied to the planar devices, it increased the average fill factor slightly and when it was used with the buckled devices it decreased it slightly.

We then began working with a conducting polymer called PEDOT:PSS which is commonly used in next generation solar cells and organic light emitting diodes as a buffer layer on top of ITO. Its use is typically meant to accomplish two things. The first is to present a more consistent surface texture to subsequent device layers (in our case CuPC) than would otherwise be present on bare ITO. The second is to provide for better potential energy alignment between ITO and subsequent layers. In solar cells this can have the impact of improving charge extraction, increasing open circuit voltage and fill factor.

To test the utility of PEDOT:PSS in our device structure we fabricated both planar and buckled substrate devices with and without PEDOT. The results of these experiments can be seen in Figure 33.

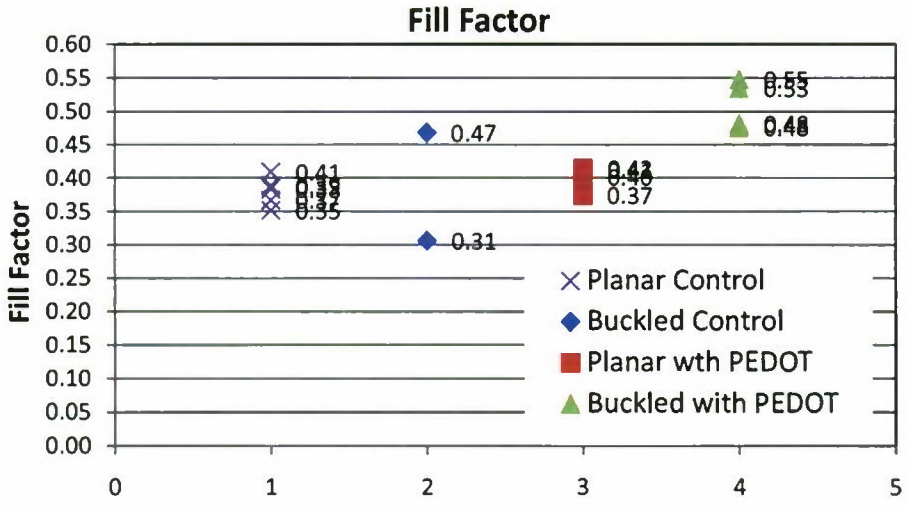

Figure 33. Results of experiments examining the impact of a PEDOT:PSS layer on the fill factor of OPV devices.

The PEDOT:PSS did not have a dramatic impact on the fill factor of the planar devices but it did improve the fill factor of the buckled substrate devices. The best buckled substrate device fill factor observed was 0.55. This compares well to the highest fill factor we observed from planar devices (during previous device runs) of 0.6 and was the highest fill factor observed for a buckled device. In this particular experiment the ITO electrodes had poorly defined edges so quantifying and comparing device current (and therefore efficiency) was not possible. But this was an encouraging result and points to further performance improvements that can be gained through continued PEDOT:PSS development work on buckled substrates.

As we continued to refine our OPV device fabrication procedures we observed a buckled substrate device that had both higher short circuit current and higher power conversion efficiency. The performance parameters are summarized in Table 5 and the I-V curves are shown in Figure 34 and Figure 35. *These results for the first time showed that a buckled substrate can be used to increase the performance of a low cost thin film solar cell.* The fill factor of 0.43 is still ~20% lower than the control device, which shows that there is potential to improve this result even further. The ISC for the control device is typical for a planar substrate, while the value of 10.3 mA/cm^2 is unusually large, even for devices on buckled substrates. More typically we have seen ISC increases for buckled substrates in the range of 30-40%. But this means that the improvement in fill factor is sufficient to result in a higher efficiency for "typical" increases in ISC due to buckling.

Table 5. Summary of performance parameters for the highest-performing devices within a group of OPV devices fabricated on planar and buckled substrates.

	Planar Control	Buckled Substrate
Isc (mA/cm^2)	6.1	10.3
Voc (V)	0.46	0.45
FF	0.57	0.43
PCE (%)	1.59	1.92

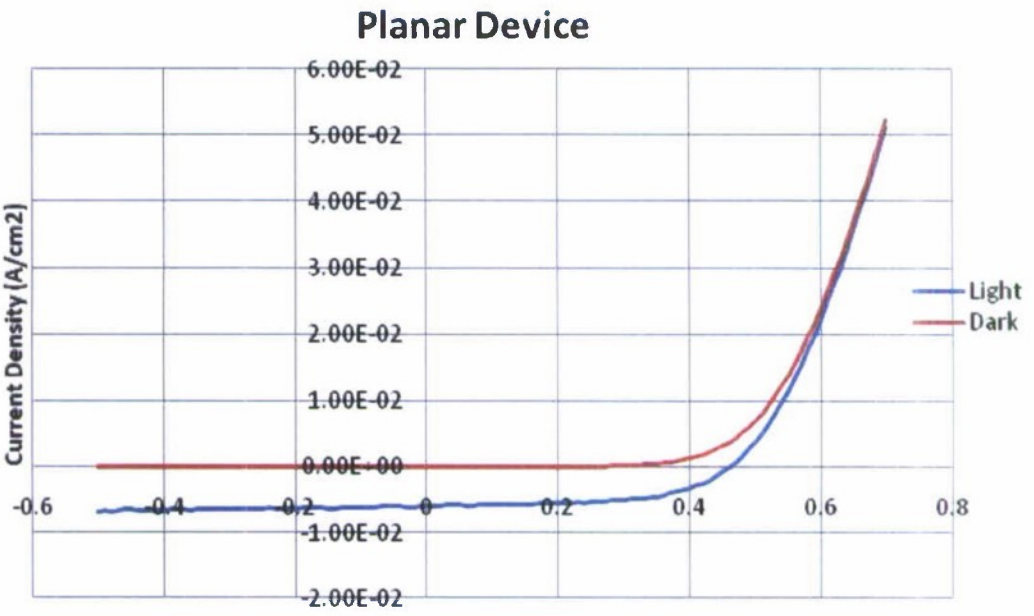

Figure 34. Light and dark current-voltage curves of a small molecule PV device fabricated on a planar crossbar substrate. The power conversion efficiency of this device was 1.59%, short circuit current was 6.1 mA/cm^2, the fill factor was 0.57 and and the open circuit voltage was 0.46V.

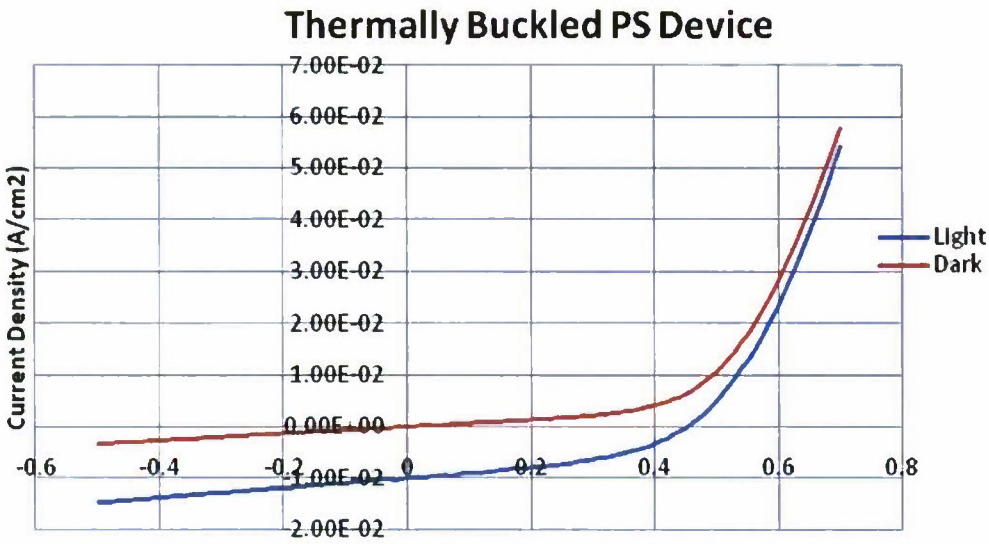

Figure 35. Light and dark current-voltage curves of a small molecule PV device fabricated on a thermally buckled crossbar substrate. *The power conversion efficiency of this device was 1.92%*, short circuit current was 10.3 mA/cm^2, the fill factor was 0.43 and and the open circuit voltage was 0.45V.

3.3 Demonstrate improved light harvesting using QDPVs

3.3.1 Highlights

- Fabricated QDPV devices which compare the performance of dot-contact and crossbar contact geometry
- Fabricated QD PV devices on expoxy-replica buckles
- Developed new fabrication methods for deposit solution processed QDs onto buckled PS substrates
- Examined performance impact of using thermally buckled PS substrates which exhibited an 11% increase in the short circuit current over a planar equivalent.
- Fabricated QDPV devices on three different types of buckled topology substrates and examined the impact that buckle aspect ratio has on optical absorption
- Measured and average optical absorption of 51% on a planar substrate and an average optical absorption of 73 and 79% on two different types of high aspect ratio scattering substrates.

The other generation thin film device technology we sought to apply to high surface topography substrates were solar devices based upon solution processed quantum dots

(QD). This effort saw us working to fabricate QDPV devices on these substrates and developing new treatment techniques to improve the electronic properties of the quantum dot layer and the solar cell performance. QDPV devices are fabricated in a similar manner to that of the OPV device with most of the device layers thermally evaporated onto the substrate. A significant difference lay in the deposition of the QD layer. In QDPV devices the QD layer is spin coated from solution onto the PV device substrate.

3.3.2 Electrical Characterization

In parallel with the development of the OPV devices we also fabricated QDPV devices on buckled substrates. The first set of device we made used a thermally buckled PS substrate and we compared its performance to a QDPV device fabricated on a planar substrate. Figure 36 shows the performance of a typical device from this first attempt and compares its performance to a device fabricated on a planar substrate. These initial device results showed that the device fabricated on a buckled substrate (i.e. "pre-buckled" rather than buckled after device fabrication) had lower short circuit current, lower fill factor, and hence lower power conversion efficiency than the planar device. This was likely due to the fact that these devices were fabricated using a dot-based (non-cross bar) architecture. As a consequence they suffered from the same contacting problems that had hampered our efforts to test OPV buckled topography devices.

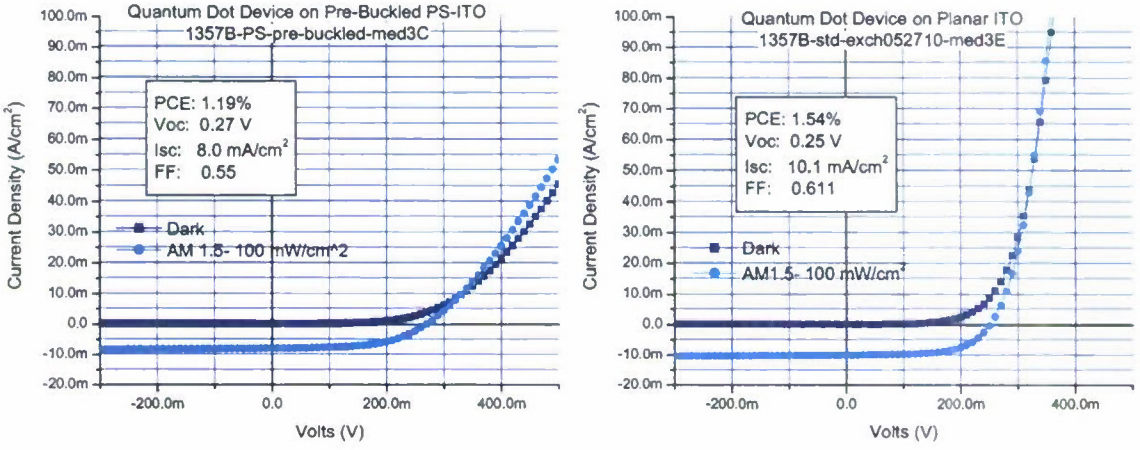

Figure 36. Current-voltage curves for QDPV devices fabricated on buckled substrates (left) and planar substrates (right).

Once the patterned crossbar substrates were completed we performed a number of QDPV device runs using patterned ITO substrates on thermally buckled PS. What we

discovered during these runs was that the solvent system used to spin coat the quantum dots had a negative impact on the PS buckles. During spin coating the solvent started to dissolve the PS which effectively destroyed the final devices. To overcome this problem we needed to change the solvent to one that would not interact with the PS buckles.

The spin coating solvent formulation we were using consisted of a mixture of octane, anisole and butylamine. When we performed experiments examining the impact these solvents have on the PS thermal buckles we found that the anisole and the butylamine were partially dissolving the polymer buckles and were responsible for the damage we had observed. Further experiments showed that we could replace the anisole and butylamine with octanol and successfully spin coat QD layers onto buckled substrates. This allowed us to fabricate QDPV devices on scattering substrates.

We deposited a QDPV device stack on three different scattering substrate types; thermally buckled polystyrene, epoxy replicas of mechanically buckled polymer, and epoxy replicas of textured Si. We started with the thermally buckled substrates and obtained functioning PV devices which we were able to compare to their planar equivalent. Typical current-voltage curves of these devices can be seen in Figure 37 and Figure 38.

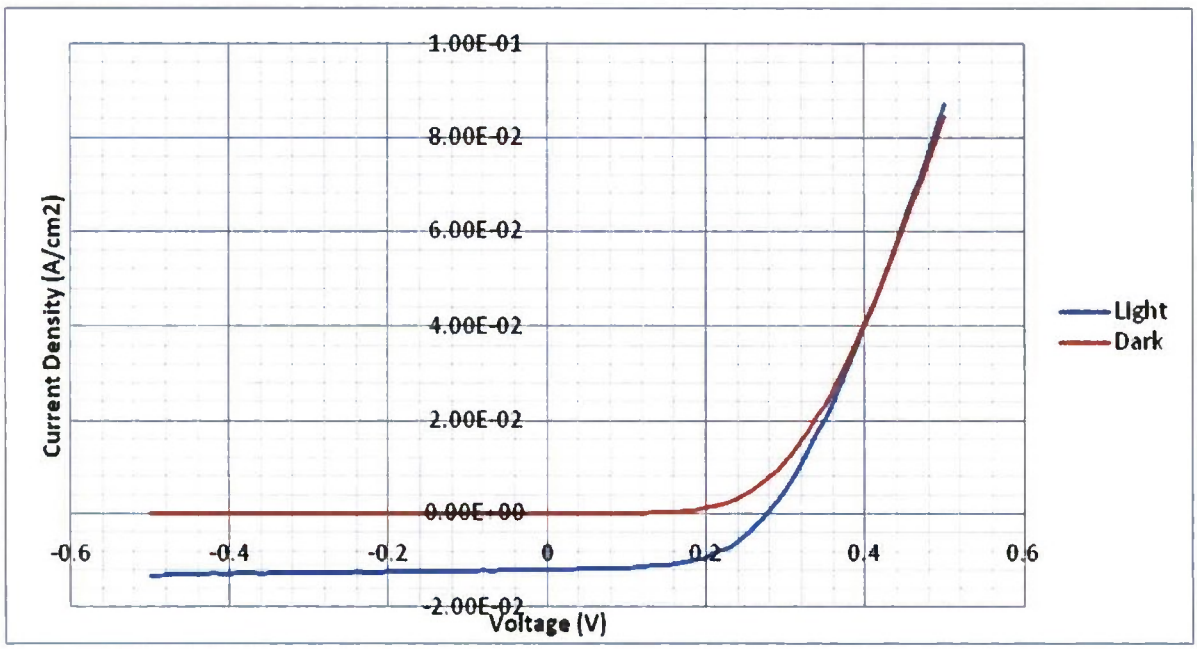

Figure 37. Current-voltage characteristics of a typical planar QDPV device during dark and light operation. The PCE of this device was 1.87%, the Voc was 0.28V, the Isc was 11.9 mA/cm^2, and the FF was 0.58.

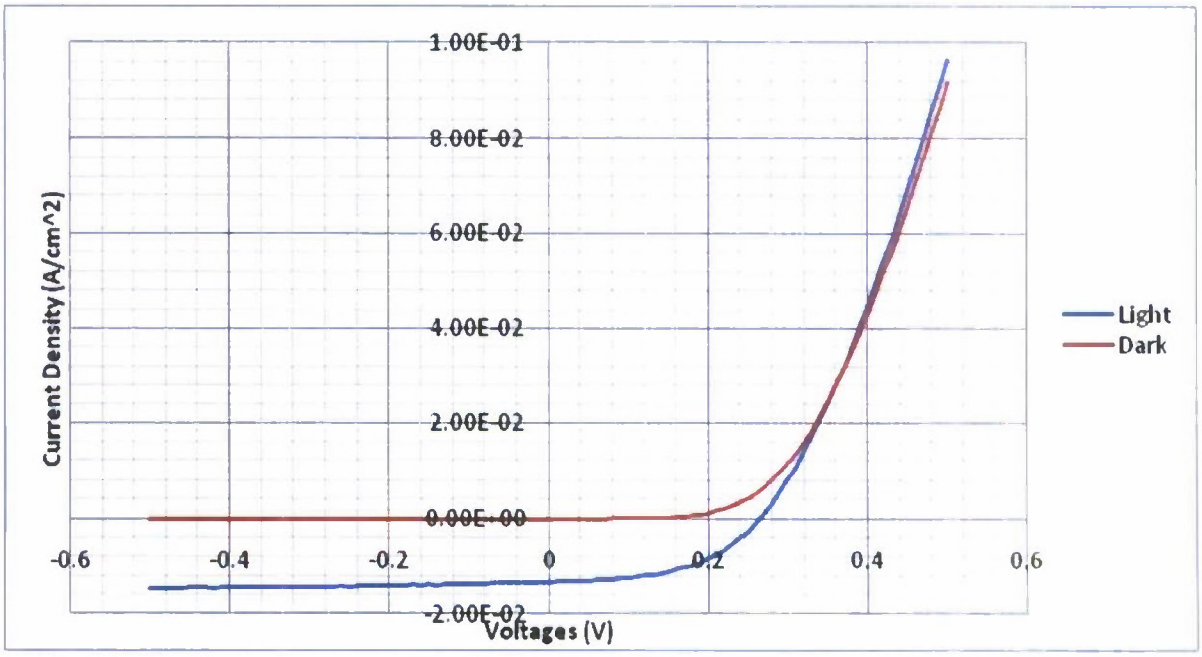

Figure 38. Current-voltage characteristics of a typical QDPV device fabricated on thermally induced PS buckles. The PCE of this device was 1.75%, the Voc was 0.26V, the Isc was 13.3 mA/cm^2, and the FF was 0.51.

We found that there was not a significant difference in the performance of the planar or thermally buckled performance although there was an 11% increase in the short circuit current of the buckled device.

3.3.3 Optical Characterization

To try to understand what impact the thermal buckles were having on the devices we examined their optical absorption as compared to the planar devices. We looked at the amount of light being reflected back from device after it passed through the entire device stack and then reflected off of its back aluminum contact. One can see the results of these measurements in Figure 39.

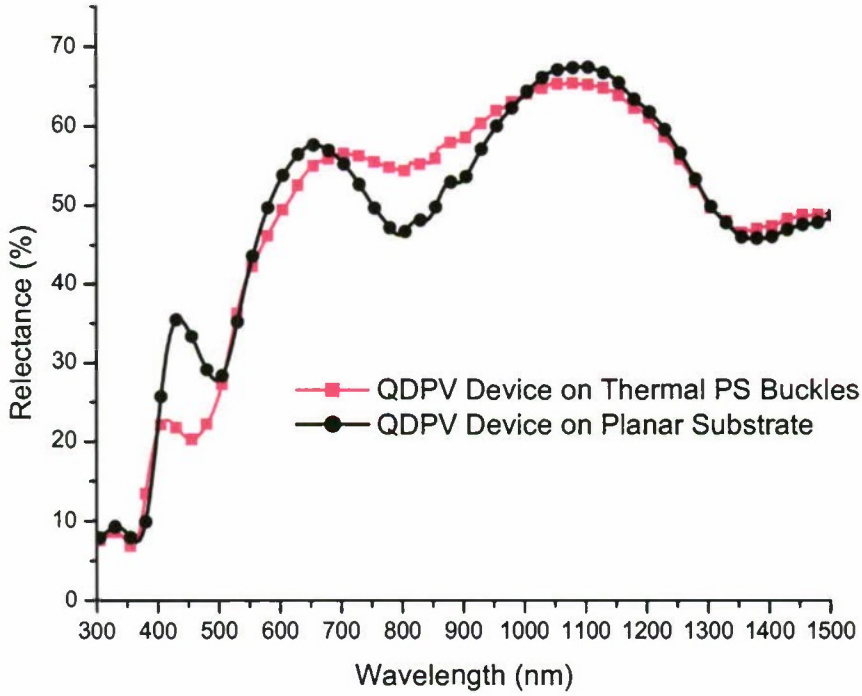

Figure 39. Spectral reflectance measured in QDPV devices fabricated on a planar and thermally induces PS buckled substrates.

The optical data in Figure 39 shows that QDPV devices fabricated on thermal buckles do not exhibit substantially higher or lower light absorption as compared to a planar device, but that there is a reduction in the magnitude of the interference oscillations in a planar device that results in more or less absorption at particular wavelengths.

We then examined the impact that larger aspect-ratio topography devices would have on optical absorption by fabricating devices on mechanically induced buckles and epoxy replicas of textured Si. Unfortunately, due to the choice of metal contact patterns these devices were not electrically functioning but they were able to allow us to examine their optical characteristics. The spectral reflectance was measured and compared to their planar equivalent and the results of these measurements can be seen in Figure 40.

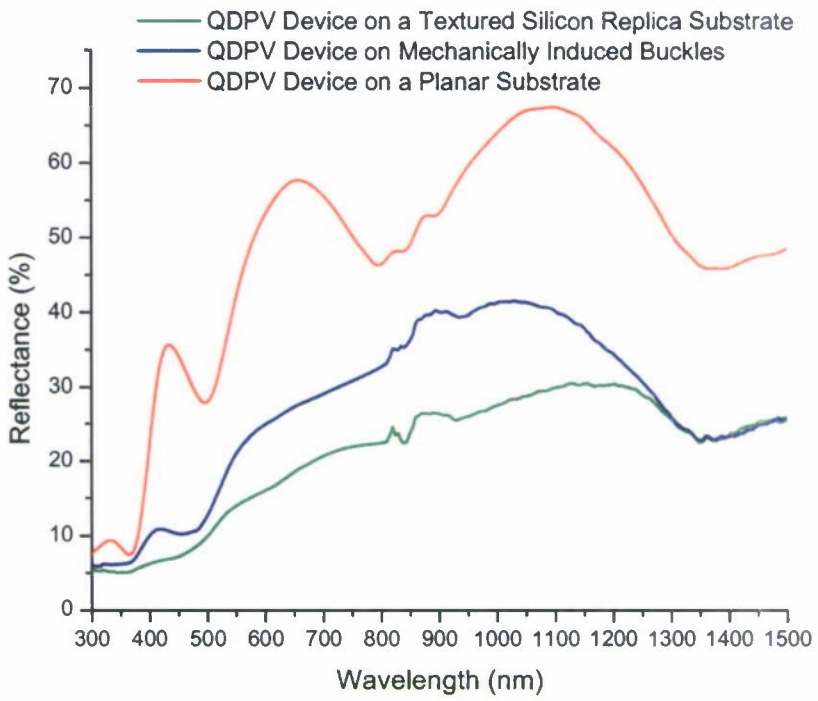

Figure 40. Spectral reflectance measured in QDPV devices fabricated on a planar, mechanically induced buckled substrate and a textured silicon replica substrate

These optical measurements show that by moving to textured substrates with higher aspect ratio topography the optical absorption of a QDPV device can be significantly enhanced. The average amount of light that is reflected back from these different substrate types was calculated across the spectral region from 300 nm to 1600 nm. The average reflectance of the planar device was 49%. The average reflectance of the mechanical buckled device was 27% and the average reflectance of the textured Si replica substrate was 21%.

These measurements lead us to the conclusion that for QDPV devices a higher aspect ratio topography than can be obtained with thermal buckles is needed to enhance optical absorption and improve PV performance.

3.4 Enhance QDPV Performance Using Chemical Methods

3.4.1 Highlights

- Explored chemical treatment/processing methods for improving performance of Quantum Dot PV devices. Air annealing increased QDPV power conversion efficiency from 1.56% to 2.24%, an increase of 43%.

We explored a number of paths for improving the performance of QDPV devices via chemical means. One such path was to examine the impact of air annealing on device performance. Air annealing was expected to chemically modify the surfaces of the QDs by introducing oxidation products (such as PbO, and $PbSO_3$). This has been shown to change the electronic properties of the QDs. Another route we explored was using a Pb-solder precursor to treat the QD films. This treatment is anticipated to increase the Pb content of the QD surfaces, which should lead to a modification of their electronic properties.

PV devices were fabricated using these treatments and compared to a standard device. The results of these experiments can be seen in Figure 41. It is important to note that the air annealing improved the performance of our standard device. This was primarily due to increases in short circuit current and fill factor. These results indicate that treatments which increase the oxide content of the QD surfaces could be further explored for improving PV device performance.

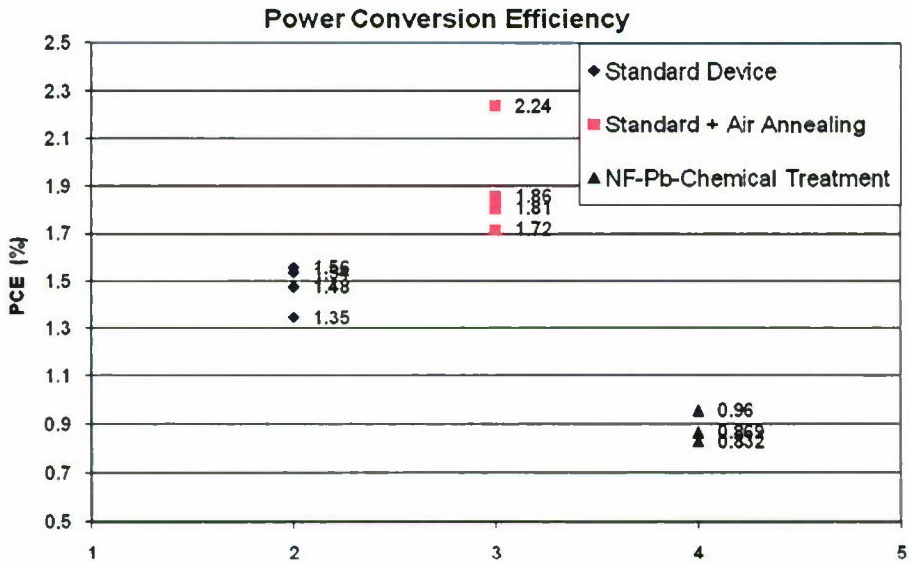

Figure 41. Impact of air annealing an NF-Pb chemical treatment on the power conversion efficiency of QDPV devices.

3.5 *Scale-up PV device size*

To demonstrate the concept of enhanced absorption through surface topography on a technologically relevant device size, we designed and fabricated devices on a larger 50 cm^2 platform. The goal was to demonstrate improved light absorption and device efficiency using a layout based on a 100 mm square glass panel with 10 sub-regions, each comprising an individual 5 cm^2 device. The individual devices could be externally configured in a parallel circuit to provide the output of a single 50 cm^2 device. However the layout allowed us to interrogate sub-regions to evaluate uniformity and single out regions that may have defects causing a high series or low shunt resistance. Figure 42 shows a drawing of the layout for which shadow masks and photomasks were subsequently produced.

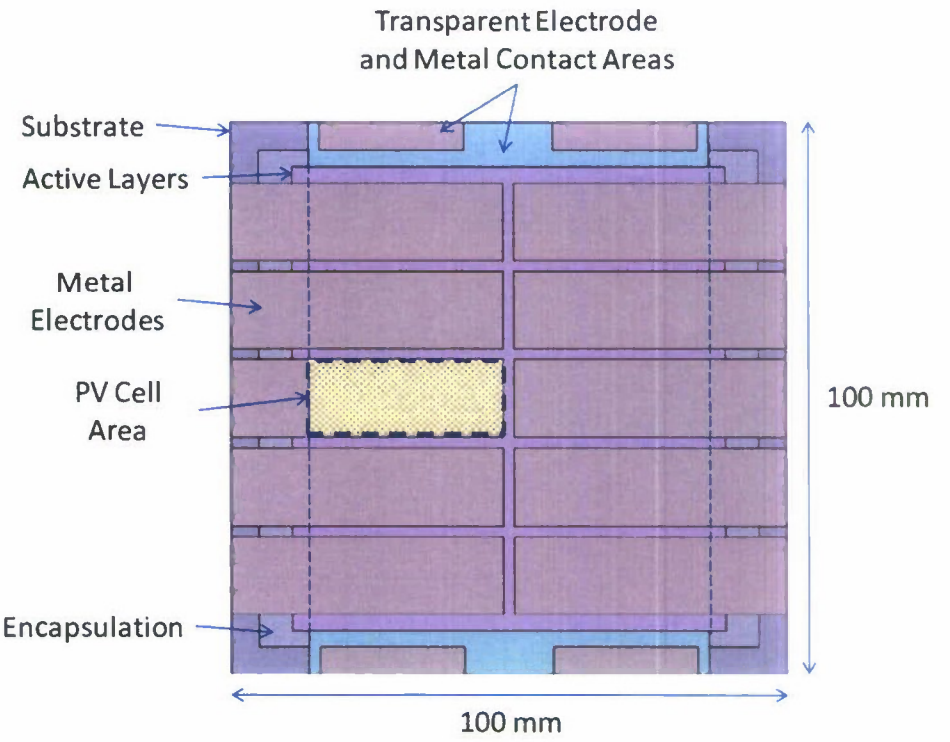

Figure 42. Schematic drawing of the 50 cm^2 device layout. The various regions are ITO (light blue), metal electrode (dark gray), active device layers (purple), encapsulation (light gray), and active device regions where the ITO and metal intersect (yellow).

A series of activities were conducted to fabricate functional arrays, outlined as follows:

- Design layout
- Fabricate substrate holder and shadow mask for ITO layer in NCSU sputter system

- Fabricate substrate holder and shadow masks for organic layers and metal layers in RTI deposition system
- Procure custom-sized glass panels for substrates and encapsulation
- Develop process for coating uniform polystyrene layers on large substrates
- Develop process for uniform ITO deposition on large substrates
- Develop process for cleaning large substrates
- Troubleshoot and correct problems with mask configuration
- Fabricate multiple batches of devices on large substrates (one substrate at a time).

Of these steps, significant effort was devoted to uniformly coating ITO on the large substrates. In a commercial deposition system, a long, narrow sputter target is typically used and a substrate moves linearly underneath the target yielding uniform coatings. In a typical research design, circular targets are used, and achieving high uniformity over areas larger than the sputter target is challenging. Ultimately excellent transparency and uniformity (>80% and <50 Ω/sq, respectively) were achieved. A second challenge was improving yield of the devices. The use of the polystyrene layer limited the traditional cleaning methods available, yet the large device area makes cleaning increasingly more critical. Second, it was found that the mask mount-demount process caused small yet sufficient damage around the edge of the devices to cause shorting of the devices.

After addressing these challenges, functional devices were successfully fabricated on both planar and buckled substrates. Unfortunately the performance of the devices was too low to adequately demonstrate or evaluate the effects of substrate topography. Table 6 gives a summary of the performance of the individual device regions for the best buckled and planar substrates, respectively. The data show that the current and fill factors are particularly low, leading to overall device efficiencies ~100x lower than the smaller devices. Improving these results would require focusing additional resources to optimizing the cleanliness of each step in the process, particularly in polystyrene coating, ITO deposition, active layer deposition, as well as in substrate transport and handling between steps. It is also not clear whether the issue with device damage from mask handling was completely resolved.

Table 6. Device performance results for each sub-region of the best planar and buckled device arrays on the large 100mm substrates.

Buckled CuPc	PCE (%)	V_{OC} (V)	I_{SC} (mA/cm^2)	FF
Dev1	0.0004	0.14	0.0022	0.264
Dev2	0.0005	0.14	0.0029	0.263
Dev3	0.0028	0.25	0.0085	0.261
Dev4	0.0058	0.34	0.0131	0.269
Dev5	0.0117	0.42	0.0213	0.261
Dev6	0.0414	0.45	0.0752	0.250
Dev7	0.0145	0.4	0.0292	0.254
Dev8	0.0068	0.34	0.0159	0.258
Dev9	0.0044	0.34	0.0103	0.254
Dev10	0.0094	0.37	0.0205	0.254
Average **(Total)**	*0.0098*	*0.32*	**0.1991**	*0.259*

Planar CuPc	PCE (%)	V_{OC} (V)	I_{SC} (mA/cm^2)	FF
Dev1	0.0080	0.13	0.0506	0.262
Dev2	0.0367	0.32	0.1016	0.233
Dev3	0.0304	0.25	0.1037	0.244
Dev4	0.0362	0.22	0.1352	0.255
Dev5	0.0279	0.14	0.1570	0.254
Dev6	0.0218	0.26	0.0693	0.241
Dev7	0.0320	0.29	0.0963	0.237
Dev8	0.0273	0.24	0.0973	0.244
Dev9	0.0425	0.29	0.1319	0.222
Dev10	0.0506	0.25	0.1741	0.242
Average **(Total)**	*0.0313*	*0.24*	**1.1170**	*0.244*

Despite the low device efficiency several interesting things were learned from these large devices. The picture in Figure 43 shows the devices from an angled perspective. From these one can see the smooth electrodes on the planar substrate on the right does not reflect the room light into the camera because it is not at the angle to catch specular reflections. However the buckled substrate on the left clearly shows the circular region where buckling occurred. Within this region room lights are diffusely scattered such that some of that light is reflected to the camera. This image shows that the buckling phenomenon is strongly influenced by the properties of the ITO film and can vary even when optical and electrical uniformity is acceptable. Still, that the circular region possesses good optical, electrical, and buckling properties shows that a production-scale tool could be optimized to produce buckled films over large areas.

While the device performance is disappointing, the large device areas offer easier optical absorption measurements with smaller influence from the optical effects from integrating spheres mentioned in previous sections. Figure 44 shows the optical absorption of the devices on planar and buckled substrates and there are several notable features. First, the planar device absorbs more efficiently in the ~600 – 720 nm absorption band of CuPc, while the buckled device is more absorbing in the ~450 – 550 nm absorption band of C_{60}, which in these devices contributes less to the photocurrent. In general terms, one absorption spectrum is not inherently better than the other, but they are significantly different. While the integrated areas of the curves are within 2% of one another, there are differences between them as high as 18%, which is more than can be achieved using traditional anti-reflective coatings. It should be noted that due to

the large device area, the nature of the buckling is different than what was seen in the smaller devices, and the regions of improved absorption are not the same. This suggests that when optimized for the regions of highest absorption and highest solar flux, substrate topography could be used to provide significant increases in photocurrent, supporting the observation of higher currents reported in previous sections.

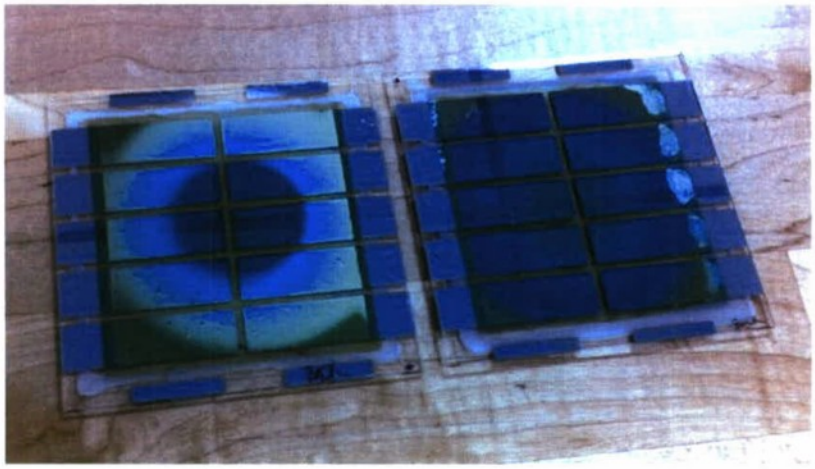

Figure 43. Photograph of device arrays on 100mm substrates with (left) and without (right) buckling.

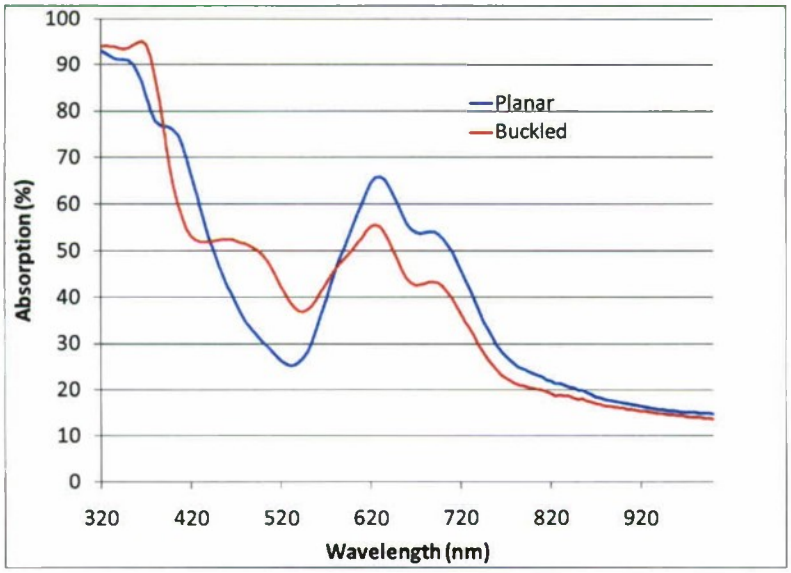

Figure 44. Absorption spectra for planar and buckled devices fabricated on large substrates with large device areas for optical measurements.

4 LIST OF SYMBOLS, ABBREVIATIONS, AND ACRONYMS

QDPV	Quantum Dot Photovoltaic
OPV	Organic Photovoltaic
PV	Photovoltaic
ITO	Indium Tin Oxide
PS	Polystyrene
C_{60}	Carbon fullerene bucky balls
CUPC	Copper phthalocyanine
BCP	Bathocuproine
UV-Vis	Ultraviolet - Visible
I-V	Current Voltage
VOC	Open Circuit Voltage
PCE	Power Conversion Efficiency
ISC	Short Circuit Current
FF	Fill Factor
PEDOT:PSS	Poly(3,4-ethylenedioxythiophene) poly(styrenesulfonate)
UVO	Ultraviolet Ozone
AM1.5G	Air mass 1.5G
DI	De-ionized